MALARIA

Malaria-driven expansion of adaptive-like functional CD56-negative NK cells correlates with clinical immunity to malaria

Maureen Ty[1], Shenghuan Sun[2]†, Perri C. Callaway[3]†, John Rek[4]†, Kathleen D. Press[1]†, Kattria van der Ploeg[1]†, Jason Nideffer[1], Zicheng Hu[2], Sandy Klemm[5], William Greenleaf[5], Michele Donato[6], Stephen Tukwasibwe[4], Emmanuel Arinaitwe[4], Felistas Nankya[4], Kenneth Musinguzi[4], Dean Andrew[7], Lauren de la Parte[1], Diego Martinez Mori[1], Savannah N. Lewis[1], Saki Takahashi[3], Isabel Rodriguez-Barraquer[3], Bryan Greenhouse[3], Catherine Blish[1,8], PJ Utz[1], Purvesh Khatri[6], Grant Dorsey[3], Moses Kamya[4,9], Michelle Boyle[7], Margaret Feeney[3,10], Isaac Ssewanyana[4], Prasanna Jagannathan[1,11]*

Natural killer (NK) cells likely play an important role in immunity to malaria, but the effect of repeated malaria on NK cell responses remains unclear. Here, we comprehensively profiled the NK cell response in a cohort of 264 Ugandan children. Repeated malaria exposure was associated with expansion of an atypical, CD56^{neg} population of NK cells that differed transcriptionally, epigenetically, and phenotypically from CD56^{dim} NK cells, including decreased expression of PLZF and the Fc receptor γ-chain, increased histone methylation, and increased protein expression of LAG-3, KIR, and LILRB1. CD56^{neg} NK cells were highly functional and displayed greater antibody-dependent cellular cytotoxicity than CD56^{dim} NK cells. Higher frequencies of CD56^{neg} NK cells were associated with protection against symptomatic malaria and high parasite densities. After marked reductions in malaria transmission, frequencies of these cells rapidly declined, suggesting that continuous exposure to *Plasmodium falciparum* is required to maintain this modified, adaptive-like NK cell subset.

INTRODUCTION

Plasmodium falciparum (*Pf*) malaria resulted in an estimated 240 million cases and 624,000 deaths in 2020, with rising morbidity observed in several highly endemic countries exacerbated by the coronavirus disease 2019 (COVID-19) pandemic (*1*). The burden of disease falls mainly on young African children, with 77% of deaths reported in African children <5 years of age. With increasing age and repeated malaria episodes, children eventually gain protection against severe disease, followed by protection against symptomatic illness. This age- and exposure-dependent clinical immunity is composed of two distinct components: "anti-parasite" immunity, or partial control of blood-stage parasite densities, and "anti-disease" immunity, or the ability to tolerate higher parasite densities without fever (*2*). However, clinical immunity is short-lived, and the precise determinants driving these distinct components of naturally acquired antimalarial immunity remain poorly understood (*3*).

Although malaria-specific antibodies likely play a key role in clinical immunity through both binding inhibition and Fc-dependent antibody effector functions (*4*–*7*), the role of the cellular immune response in clinical immunity is less clear. Innate immune cells can recognize and respond to *Plasmodium* parasites (*8*, *9*), but pathogen-induced production of inflammatory cytokines by these cells has also been implicated in the pathogenesis of symptomatic and severe malaria (*8*–*10*). The development of naturally acquired immunity likely involves the careful regulation of the innate immune response to limit the negative consequences of inflammation while partially controlling parasitemia. Recent studies have suggested that exposure to malaria may modify several innate immune cells (*11*–*15*), potentially through transcriptional and epigenetic reprogramming (*13*, *16*, *17*). Whether malaria-induced innate immune modulation plays a role in driving and/or maintaining clinical immunity is unknown.

Natural killer (NK) cells have increasingly been recognized as key players in the host immune response to malaria through both direct parasite recognition (*18*) and antibody-dependent cellular cytotoxicity (ADCC) (*7*) (*19*). These cells have traditionally been divided into subsets on the basis of expression of CD56 and CD16, with CD56^{dim}CD16^{+} NK cells typically comprising most of the NK population in peripheral blood, although the complexity and diversity of NK cell subsets have only recently been interrogated using single-cell approaches (*20*–*22*). A subset of CD56^{dim} NK cells with low expression of the transcription factor promyelocytic leukemia zinc finger (PLZF) and the signaling Fc receptor γ-chain (FcRγ) was found to have enhanced ADCC against *Pf*-infected red blood cells (iRBCs) and was associated with resistance to symptomatic malaria in Malian children (*23*). It remains unclear whether repeated malaria drives expansion of this "adaptive-like" NK cell subset or whether these cells are maintained stably in the absence of

[1]Department of Medicine, Stanford University, Stanford, CA, USA. [2]Bakar Computational Health Sciences Institute, University of California, San Francisco, San Francisco, CA, USA. [3]Department of Medicine, University of California, San Francisco, San Francisco, CA, USA. [4]Infectious Diseases Research Collaboration, Kampala, Uganda. [5]Department of Genetics, Stanford University, Stanford, CA, USA. [6]Institute for Immunity, Transplantation, and Infection, Stanford University, Stanford, CA, USA. [7]Queensland Institute for Medical Research, Queensland, Australia. [8]Chan Zuckerberg Biohub, San Francisco, CA, USA. [9]Department of Medicine, Makerere University, Kampala, Uganda. [10]Department of Pediatrics, University of California, San Francisco, San Francisco, CA, USA. [11]Department of Microbiology and Immunology, Stanford University, Stanford, CA, USA.
†These authors contributed equally to this work.
*Corresponding author. Email: prasj@stanford.edu

continuous exposure to malaria parasites. Some reports have also described a subset of CD56^{neg} CD16^{+} NK cells that are expanded in the context of chronic viral infections such as HIV (*24*) and hepatitis C virus (HCV) (*25*), as well as among patients with acute myelogenous lymphoma (AML) (*26*) and malaria-exposed African children with Epstein-Barr virus (EBV)–related Burkitt's lymphoma (*27*). Given a reduced capacity of these cells to produce cytokines in response to stimulation, some suggest that these cells may represent a dysfunctional and/or exhausted phenotype (*26*, *28*). Whether CD56^{neg} NK cells expand after repeated malaria, have functional capabilities, and/or play a role in clinical immunity to malaria is unknown.

In this study, we characterized the NK cell response among 264 children followed in the East African International Centers of Excellence in Malaria Research (ICEMR) cohorts in Eastern Uganda. We used multiparameter flow cytometry, cellular indexing of transcriptomes and epitopes by sequencing (CITE-seq), epigenetic profiling using cytometry by time of flight (EpiTOF), and assay for transposase-accessible chromatin using sequencing (ATAC-seq), along with functional assays, to comprehensively profile NK cell responses. We demonstrate that repeated malaria exposure is associated with expansion of highly functional CD56^{neg} NK cells that strongly correlate with acquisition of clinical immunity to malaria. However, in the absence of continuous malaria exposure, frequencies and function of these cells rapidly decline.

RESULTS

Increasing exposure to malaria is associated with higher frequencies of CD3^{-} CD7^{+} CD56^{neg} NK cells

We analyzed circulating NK cell populations from peripheral blood mononuclear cells (PBMCs) collected in 2013 among 45 children ages 3 to 7 living in two districts in Eastern Uganda with very different malaria transmission intensities: Jinja, with an estimated annual entomological inoculation rate (aEIR) of 2.8 infectious bites per person per year, and Tororo, with an aEIR of 310 infectious bites per person year (*29*). Nearly all children were human cytomegalovirus (HCMV) positive at the time of sampling (table S1). CD3^{-}, CD14^{-}, CD19^{-}, CD7^{+} NK cells were classified by the expression of CD56 and CD16 into three subsets: CD56^{bright} (CD56^{+} CD16^{-}), CD56^{dim} (CD56^{dim} CD16^{+}), and CD56^{neg} (CD56^{neg} CD16^{+}) (Fig. 1A and fig. S1). Children living in the highly endemic Tororo district had significantly lower frequencies of CD56^{dim} NK cells ($P = 5.6 \times 10^{-5}$) and higher frequencies of CD56^{neg} NK cells ($P = 1.3 \times 10^{-5}$) than age-matched Jinja children (Fig. 1B and table S1). Percentages of CD56^{neg} NK cells positively correlated with household-level aEIR, a direct measurement of exposure to *Pf*-infective mosquitoes ($P = 2.5 \times 10^{-6}$, Fig. 1C). We correlated frequencies of NK cell subsets with age, a surrogate for cumulative malaria exposure in high transmission settings, among a larger Tororo cohort of 242 children ages 6 months to 10 years (table S2). We found that increasing age was associated with increasing frequencies of CD56^{neg} NK cells ($P = 1 \times 10^{-6}$) and decreasing frequencies of CD56^{dim} NK cells ($P = 1 \times 10^{-4}$; Fig. 1D). Together, these data suggest that CD56^{neg} NK cells are increased in children repeatedly exposed to malaria.

Single-cell RNA sequencing reveals that CD56^{neg} NK cells have transcriptional features of both "adaptive" and "exhausted" NK cells

To further characterize NK cells at the single cell level, we used CITE-seq, a method of single-cell RNA sequencing that simultaneously assesses DNA-barcoded antibodies against cell surface proteins. PBMCs from 10 independent Tororo participant samples were analyzed (n = 60,381 total cells; table S3). Unsupervised clustering of RNA transcripts using uniform manifold approximation and projection (UMAP) revealed that NK cells cluster near T cells, with CD8^{+} T cells as the closest neighbors (Fig. 2A). Using cell surface protein tags for CD56 and CD16, we identified three distinct cell subsets within the CD19^{-}, CD3^{-}, CD14^{-} CD7^{+} NK cell population (Fig. 2B) and visualized these cell populations on the RNA UMAP projection. CD56^{dim} and CD56^{neg} NK cells were both identified in the same NK cell RNA cluster, suggesting transcriptional similarities between these subsets (Fig. 2C and fig. S2A). However, we also identified gene transcripts differently enriched in each subset (Fig. 2D). In comparison with CD56^{dim} NK cells, CD56^{neg} cells had significantly lower expression of *ZBTB16* (P = 0.001), which encodes the transcription factor PLZF, and *FCER1G* ($P = 2.2 \times 10^{-25}$), which encodes the FcRγ signaling receptor (Fig. 2E, top row). Conversely, CD56^{neg} NK cells had higher expression of *BC11B* ($P = 2.3 \times 10^{-6}$), a transcription factor shown to repress PLZF (*30*) (Fig. 2E). Expression of PLZF and FcRγ is decreased in adaptive-like NK cells with enhanced capacity for ADCC (*22*, *23*). CD56^{neg} NK cells had lower expression of genes encoding the cell surface markers *KLRB1* (CD161, $P = 5.7 \times 10^{-15}$) and *KLRF1* (NKp80, $P = 2.8 \times 10^{-22}$) and higher expression of *CD3G* ($P = 1.6 \times 10^{-11}$) than CD56^{dim} NK cells, also consistent with an adaptive-like NK cell phenotype (*22*, *31*). CD56^{neg} NK cells had lower expression of *IL-18RAP* ($P = 6.1 \times 10^{-7}$), which encodes the interleukin-18 (IL-18) receptor accessory protein and mediates IL-18–dependent signal transduction and downstream nuclear factor κB (NF-κB) activation and interferon-γ (IFN-γ) induction (*32*). CD56^{neg} NK cells also had higher expression of *LAG3* ($P = 4.2 \times 10^{-7}$), a checkpoint inhibitor that is induced by type I IFN (*33*) and chronic in vitro stimulation (*34*), and is a negative regulator of cytokine production in mature NK cells, suggestive of an exhausted phenotype (*34*, *35*). Expression of killer cell immunoglobulin-like receptor (KIR) genes was similar between CD56^{dim} and CD56^{neg} NK cells, consistent with another published report (*36*), although KIR genes were not well represented in the dataset (fig. S2B). Together, these data suggest that CD56^{neg} NK cells from malaria-exposed Ugandan children have transcriptional features suggestive of both adaptive-like and exhausted NK cells.

CD56^{neg} NK cells from Ugandan children express higher levels of LILRB1 and KIRs and differ epigenetically from CD56^{dim} NK cells

We next compared protein expression between CD56^{dim} and CD56^{neg} subsets from samples collected from 35 Tororo children (table S4). We initially focused on markers that have been implicated in NK cell differentiation (*37*) and/or adaptive NK cells (*38*) using flow cytometry, including cell surface receptors LILRB1 (CD85J), NKG2A, NKG2C, CD57, and NKG2C, as well as intracellular signaling receptor FcRγ. Consistent with our transcriptomic data, CD56^{neg} NK cells in Tororo children had significantly reduced expression of FcRγ compared with CD56^{dim} NK cells

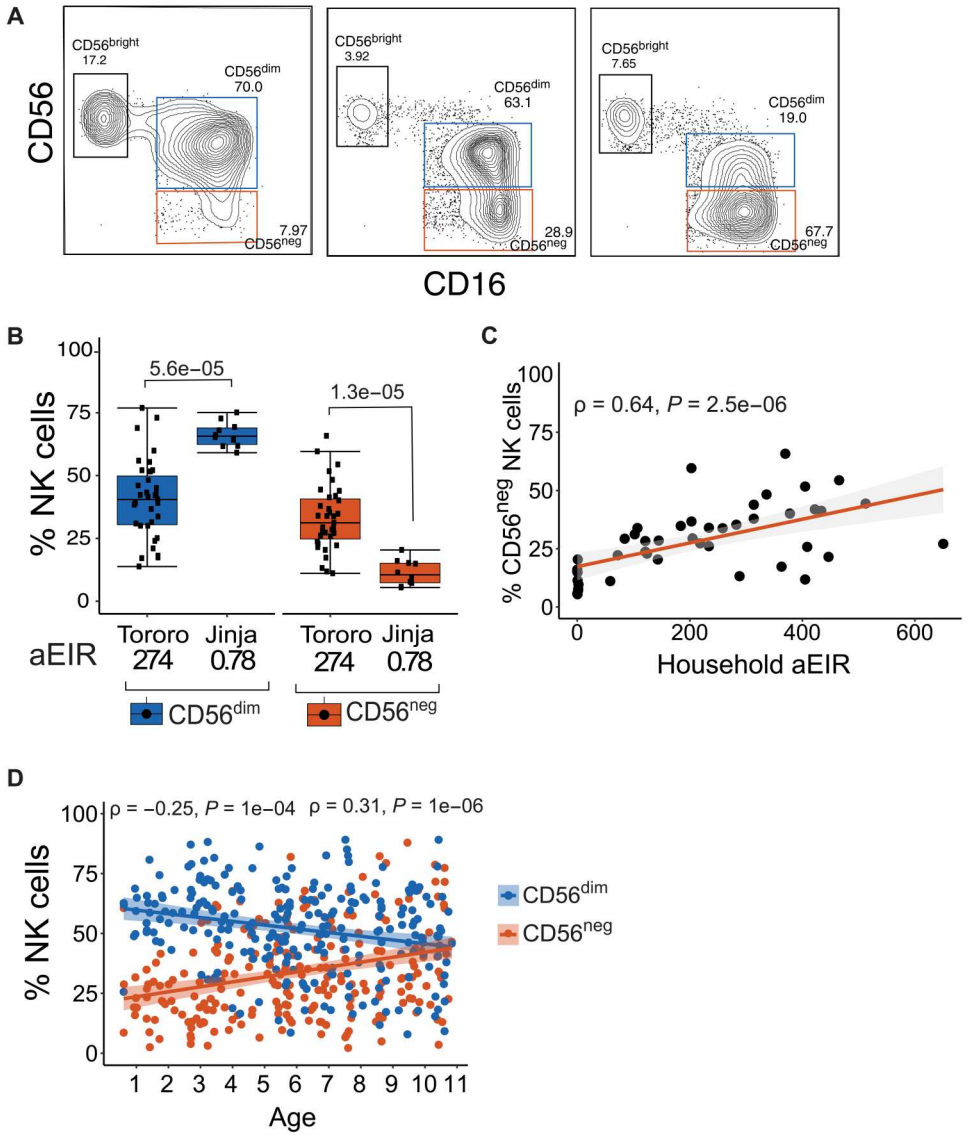

Fig. 1. Ugandan children living in high transmission settings have high frequencies of atypical CD56^{neg} NK cells. (**A**) Representative flow cytometry plots of CD3$^-$ CD14$^-$ CD19$^-$ CD7$^+$ NK cells from three children, as defined by CD56 and CD16 (fig. S1 for full gating). (**B**) Percentages of CD56^{dim} and CD56^{neg} NK cells from children ages 3 to 7 years in Tororo (n = 35) and Jinja (n = 10). Household annual entomological inoculation rate (aEIR) is an estimate of the number of infective bites received in the year before sampling across each cohort, as measured via CDC light traps (see Materials and Methods). (**C**) Correlation between CD56^{neg} NK cells and measured household aEIR among children assayed in (B). (**D**) Correlation between NK cell frequencies and age among 242 Tororo children ages 0.6 to 11 years. P values shown above box plots are calculated using Wilcoxon signed rank test, whereas the rho (ρ) and P values associated with the scatterplots are calculated using Spearman's correlation. Shaded areas represent 95% confidence interval of best-fit regression line. All samples were collected in 2013; see tables S1 and S2 for patient characteristics.

($P = 2.9 \times 10^{-5}$). In addition, CD56^{neg} NK cells also had reduced protein expression of NKG2A ($P = 4.5 \times 10^{-6}$), CD57 ($P = 0.0024$), and NKG2C ($P = 2.2 \times 10^{-4}$), but higher levels of LILRB1 ($P = 2.4 \times 10^{-7}$), compared with CD56^{dim} NK cells (Fig. 3A). We examined the combination of these markers and found that most of the CD56^{neg} NK cells are LILRB1$^+$, FcRγ$^-$, NKG2A$^-$, and CD57$^-$, whereas CD56^{dim} NK cells are most likely to be FcRγ$^+$ and NKG2A$^+$, but LILRB1$^-$ and CD57$^-$ (Fig. 3B and fig. S3). This phenotypic description of CD56^{neg} NK cells is consistent with similar cell populations within the context of chronic viral infections such as HIV (*24*). Cell surface expression of KIR2DL1 was similar between CD56^{neg} cells and CD56^{dim} cells, consistent with gene expression data. However, flow cytometric analysis revealed greater cell surface expression of the KIRs KIR3DL1 ($P = 1.5 \times 10^{-6}$) and KIR2DL2/L3/S2 ($P = 0.05$) in CD56^{neg} NK cells compared with CD56^{dim} cells (Fig. 3C), consistent with other reports that have observed increased KIR protein expression on CD56^{neg} NK cells (*24*). In addition, we confirmed other differences seen in our gene expression data, including greater LAG3 expression ($P = 0.0078$) and lower granulysin ($P = 0.049$), among CD56^{neg} compared with CD56^{dim} cells (Fig. 3D).

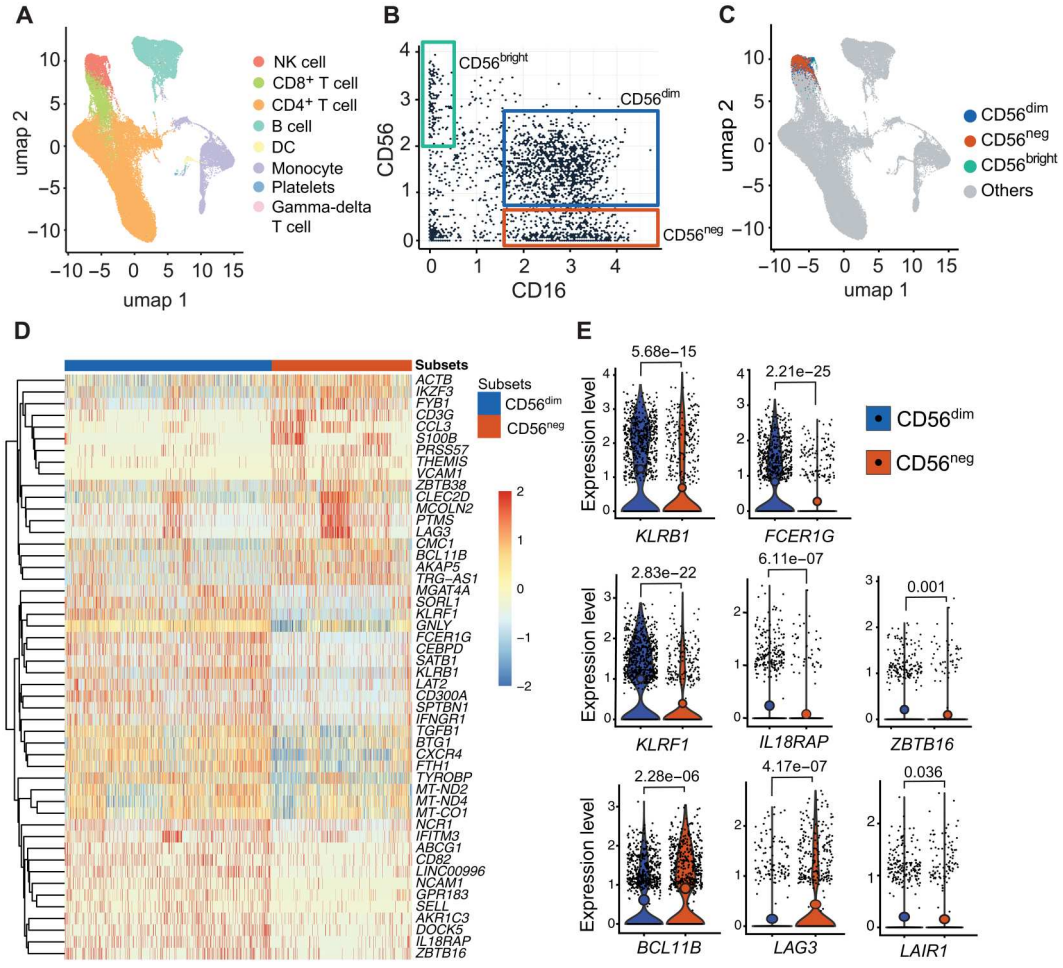

Fig. 2. Single-cell RNA sequencing of NK cells reveals transcriptional similarities and differences between CD56^{dim} and CD56^{neg} NK cells. (**A**) Gene transcripts of n = 60,381 PBMCs were clustered using Leiden algorithm and visualized in two dimensions with UMAP. (**B**) Gating of NK cell subsets as defined by surface marker expression of CD16 (x axis) and CD56 (y axis). (**C**) NK cell subsets classified by (B) superimposed with UMAP gene transcript data. CD56^{dim} transcripts are in blue, CD56^{neg} transcripts are in red, CD56^{bright} transcripts are in green, and non-NK cell transcripts are in gray. (**D**) Heatmap showing top 50 genes differentially expressed by CD56^{dim} and CD56^{neg} NK cells. (**E**) Representative violin plots comparing gene transcripts between CD56^{dim} and CD56^{neg} NK cells. P values obtained from likelihood ratio tests as implemented in the Seurat R package. Samples are from 10 individuals; see table S3 for patient characteristics.

Epigenetic differences in NK cells, including both genome-wide DNA hypomethylation and hypermethylation, have been previously shown to differentiate NK cell subsets, including adaptive NK cells (*34*, *38*). We compared global histone modifications at the single-cell level between CD56^{dim} and CD56^{neg} NK cells using EpiTOF, because these modifications have previously been shown to differentiate CD56^{bright} and CD56^{dim} NK cells (*39*). Compared with CD56^{dim} NK cells, CD56^{neg} cells had greater abundance of a number of methylation marks, including dimethylation and trimethylation of histone H3 lysine 4 (H3K4me2 and H3K4me3) (Fig. 3E), marks that are associated with gene expression in mature, aging cells (*40*). Together, these data suggest that CD56^{neg} NK cells in malaria-exposed Ugandan children have phenotypic and epigenetic features of mature, adaptive-like NK cells that differentiate them from CD56^{dim} cells.

CD56^{neg} NK cells display greater ADCC than CD56^{dim} NK cells

Having demonstrated that CD56^{neg} NK cells were transcriptionally, phenotypically, and epigenetically distinct from CD56^{dim} NK cells, we next compared their functional abilities. After a short in vitro stimulation with *Pf* iRBCs, neither CD56^{dim} nor CD56^{neg} NK cells produced significant amounts of IFN-γ (Fig. 4A). However, after IL-12/IL-15/IL-18 stimulation, CD56^{neg} NK cells produced significantly less IFN-γ in comparison with CD56^{dim} cells ($P = 6.6 \times 10^{-9}$). This result was expected given CITE-seq data showing decreased expression of *IL-18RAP* on CD56^{neg} compared with CD56^{dim} NK cells, consistent with prior reports (*28*).

We next tested whether there were differences between CD56^{dim} or CD56^{neg} NK cells in response to antibody-opsonized target cells. We stimulated PBMCs obtained from Tororo children with iRBCs alone, iRBCs incubated with plasma pooled from either malaria-naïve adults or immune Ugandan adults, or, as a positive control, iRBCs incubated with anti-RBC antibodies. In response to iRBC

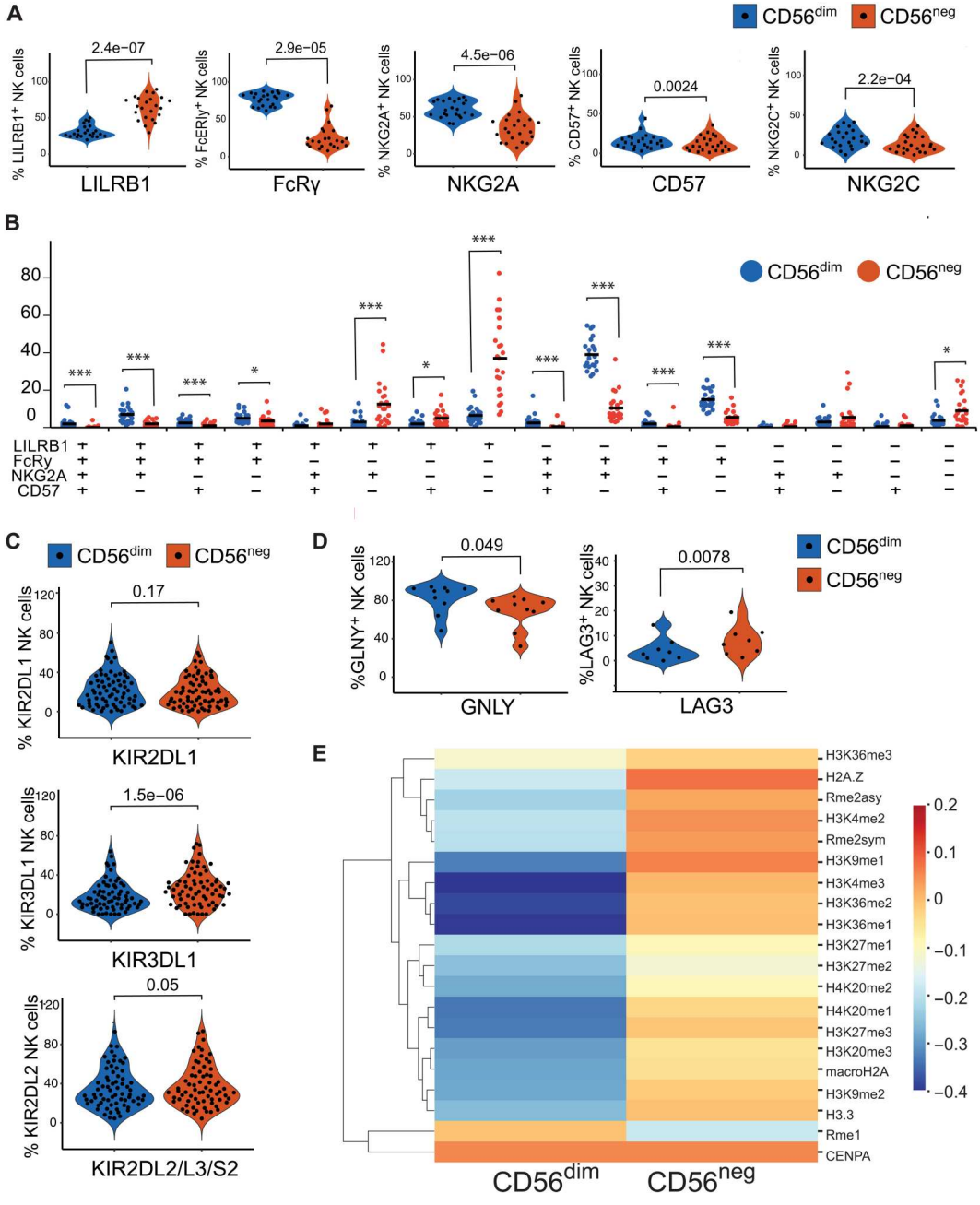

Fig. 3. Cellular phenotyping reveals CD56^{neg} NK cells to have a mature phenotype. NK cells were gated for LILRB1, FcRγ, NKG2A, CD57, and NKG2C. (**A**) Frequencies of cells are shown in violin plots. (**B**) Proportions of cells expressing all four possible marker combinations are shown in dot plots. (**C** and **D**) Percentages of NK cells expressing KIRs, granulysin, and LAG3. (**E**) Heatmap comparing distinct histone modifications between CD56^{dim} and CD56^{neg} NK cells as measured by EpiTOF from 36 participant samples. *P* values shown above violin and dot plots are calculated using Wilcoxon matched-pairs signed rank test. See table S4 for number of samples and patient characteristics, figs. S1 and S3 for gating strategies, and data file S2 for raw data.

incubated with plasma from immune Ugandan adults, CD56^{neg} NK cells produced significantly more IFN-γ ($P = 4.9 \times 10^{-5}$) and had greater degranulation (as measured by CD107a, $P = 2.4 \times 10^{-7}$) in comparison with CD56^{dim} NK cells, suggesting a heightened capacity to perform ADCC (Fig. 4, B and C). After stimulation with iRBCs alone, iRBCs treated with plasma from malaria-naïve adults, or uninfected RBCs incubated with plasma from immune Ugandan adults, neither CD56^{dim} nor CD56^{neg} NK cells produced IFN-γ or degranulated (Fig. 4, B and C, and fig. S4), indicating that the observed responses were truly antibody dependent.

To determine whether malaria-specific NK cell degranulation was independent of other cells, we isolated NK cells from 15 Tororo children by magnetic purification and performed the same ADCC assay. Again, isolated NK cells degranulated more when stimulated with iRBCs incubated with pooled plasma from Ugandan adults versus iRBCs incubated with U.S. control plasma

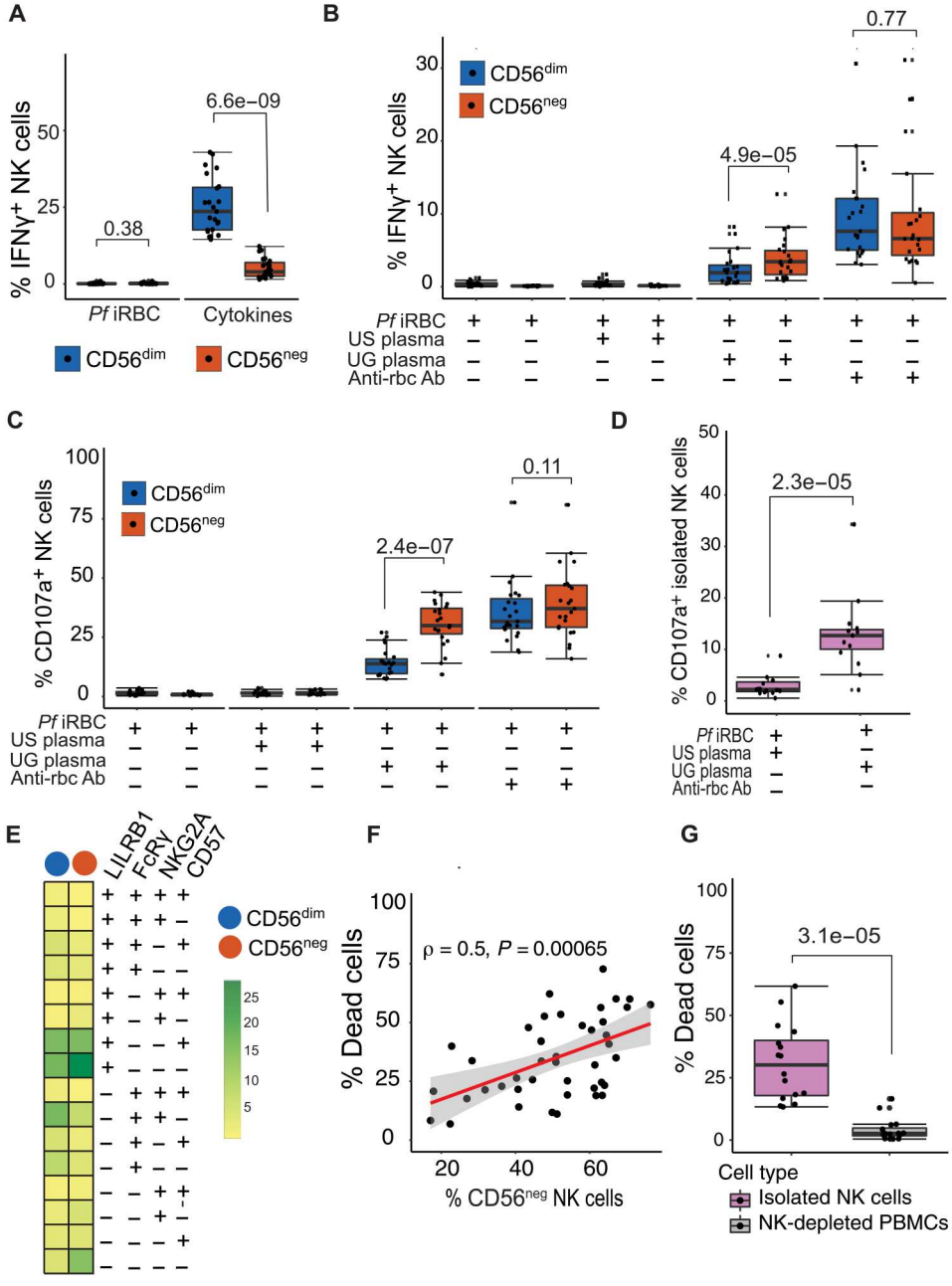

Fig. 4. CD56^{neg} NK cells have an enhanced ability for antibody-dependent cellular cytotoxicity. (**A**) PBMCs were stimulated with iRBCs or cytokines: IL-12 (2 ng/ml), IL-15 (10 ng/ml), and IL-18 (0.25 μg/ml) for 4 hours, after which intracellular IFN-γ was measured. (**B** and **C**) PBMCs were stimulated with either iRBCs alone or opsonized with serum in a ratio of 2 PBMCs to 1 iRBC. (B) IFN-γ was measured intracellularly. (C) NK cell degranulation was measured by CD107a expression. (**D**) Isolated NK cells were stimulated with iRBCs opsonized by either U.S. or Ugandan serum, and degranulation was measured. (**E**) Heatplot showing percentages of NK cells expressing cell surface markers degranulating in response to iRBCs opsonized by Ugandan serum. (**F**) Association between frequencies of CD56^{neg} NK cells and percentage of dead opsonized p815 cells. (**G**) Isolated NK cells and NK-depleted PBMCs were stimulated with opsonized p815, after which the percentage of dead cells was measured by 7-AAD staining. *P* values for box plots are calculated using Wilcoxon matched-pairs signed rank test, and rho (ρ) and *P* value associated with the scatterplot were calculated using Spearman's correlation. See table S4 for patient characteristics and data file S2 for raw data.

($P = 2.3 \times 10^{-5}$; Fig. 4D and fig. S1). Most of the degranulating CD107a^{+} NK cells after stimulation with Ugandan plasma–opsonized parasites were FcRγ^{-}, LILRB1^{+}, NKG2A^{-}, and CD57^{-} (Fig. 4E), which represent the major fraction of circulating CD56^{neg} NK cells (Fig. 3B). Other NK cell populations that degranulated also lacked expression of FcRγ (Fig. 4E), including those that were CD56^{dim}, consistent with other studies showing that FcRγ^{-} CD56^{dim} NK cells show enhanced degranulation to antibody-coated targets (*23*, *41*).

As an alternative measure of ADCC, we assessed the ability of NK cells to kill antibody-coated p815 cells (fig. S5A). After stimulation with antibody-coated p815 cells, we observed a strong positive correlation between frequencies of CD56^{neg} NK cells and p815 killing ($P = 0.00065$; Fig. 4F and fig. S5B). We further isolated NK cells and show that these cells are the main cell type that kills antibody-opsonized p815 compared with PBMCs that were depleted of NK cells (Fig. 4G). Together, these results demonstrate that malaria-induced CD56^{neg} NK cells have enhanced ADCC capacity compared with CD56^{dim} NK cells.

Higher frequencies of CD56^{neg} NK cells are associated with protection against subsequent parasitemia and symptoms of malaria

To determine the clinical relevance of these observations, we assessed associations between NK cell percentages and (i) parasite densities in the year after the cellular measurement (anti-parasite immunity) and (ii) the probability of symptoms given *Plasmodium* infection in the subsequent year (anti-disease immunity). Higher percentages of CD56^{neg} NK cells were associated with significantly lower parasite densities in the year after analysis ($P = 1 \times 10^{-10}$; Fig. 5A). In contrast, higher percentages of CD56^{dim} NK cells were associated with significantly higher parasite densities ($P = 1 \times 10^{-8}$; Fig. 5A). When considering the odds of symptoms given *Plasmodium* infection, higher percentages of CD56^{neg} NK cells were also associated with a lower odds of being symptomatic if infected (Fig. 5B and fig. S6). After adjustment for age and household aEIR, children in the highest tertile of CD56^{neg} NK cells had 71% lower odds of being symptomatic if infected in the subsequent year compared with children in the lowest tertile [adjusted odds ratio (aOR), 0.29; 95% confidence interval, 0.13 to 0.63; $P = 0.002$; Fig. 5B]. In contrast, higher percentages of CD56^{dim} NK cells were associated with higher odds of symptoms given infection (aOR, 3.88, comparing highest versus lowest tertile of CD56^{dim} NK cells; 95% confidence interval, 1.9 to 8.1; $P < 0.001$; Fig. 5B and fig. S6). Together, these data suggest that higher frequencies of CD56^{neg} NK cells, and inversion of the circulating CD56^{dim} to CD56^{neg} ratio, are strongly associated with both anti-parasite and anti-disease immunity to malaria in Ugandan children.

CD56^{neg} NK cells decline in the setting of reduced malaria transmission

Having shown that functional CD56^{neg} NK cells are increased in children repeatedly exposed to malaria, we wanted to determine whether malaria exposure was required to maintain their phenotype and function. We took advantage of a natural experiment in our Tororo cohort where children were followed both before and after initiation of an indoor residual spraying of insecticide (IRS) campaign (*42*). Before initiation of IRS in December 2014, malaria transmission was high and stable in Tororo (*29*). After initiation of IRS, malaria transmission, parasite prevalence, and malaria incidence markedly declined, and by 2018, the burden of malaria was reduced to very low transmission levels (Fig. 6A) (*42*). We assessed the stability of NK cell phenotypes over time by performing longitudinal assessments in 15 Tororo children before (August to November 2013) and after (May to October 2015) the first round of IRS (fig. S7A) and compared these with a group of 12 similarly aged children sampled in 2018, 4 years after initiation of IRS, when transmission was very low. Household aEIR among sampled participants declined from 277 in 2013 to 34 in 2015 to 1 in 2018 (table S5). The percentage of CD56^{neg} NK cells significantly decreased from the pre- to post-IRS period (median, 55.2% in 2013 versus 44.6% in 2015; $P = 0.0021$; Fig. 6B), with a concurrent increase of CD56^{dim} cells (Fig. 6, B and C), and these percentages correlated with household aEIR (fig. S7B). Percentages of CD56^{neg} NK cells were significantly lower in similarly aged children sampled in 2018 (median, 10.2% CD56^{neg} NK cells; $P = 2 \times 10^{-5}$, comparing 2018 versus 2015), when transmission and malaria prevalence were markedly lower (Fig. 6, B and C). Phenotypically, CD56^{dim} NK cells

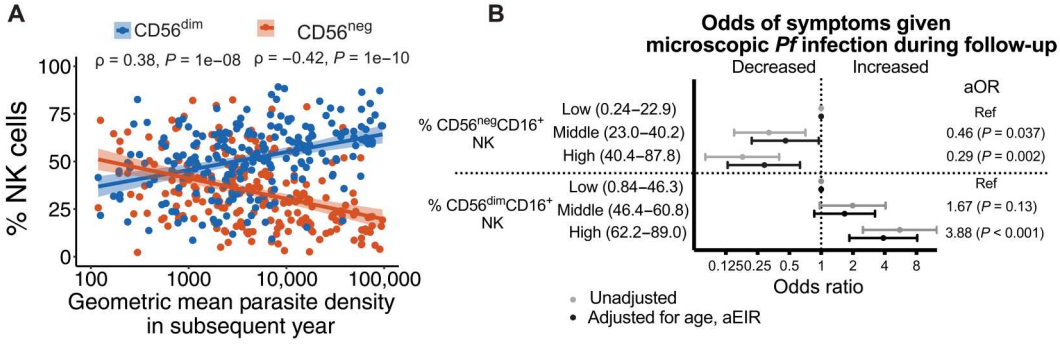

Fig. 5. CD56^{neg} NK cells are associated with clinical malaria protection. Associations between CD56^{dim} and CD56^{neg} percentages and (**A**) geometric mean parasite densities in the subsequent year. Rho (ρ) and *P* values associated with the scatterplot were calculated using Spearman's correlation. Shaded areas represent 95% confidence interval of best-fit regression line. (**B**) Associations between CD56^{dim} and CD56^{neg} percentages and probability of symptoms given *Pf* parasitemia in the subsequent year (see fig. S5 for smoothed relationships). Multilevel mixed-effects linear models used to calculate odds of symptoms given microscopic *Pf* infection (B). Multivariate models adjusted for age and aEIR and account for clustering by individual and household. Categories represent tertiles of NK response ($n = 80$, 81, and 81 per tertile). aOR, adjusted odds ratio. See table S2 for patient characteristics.

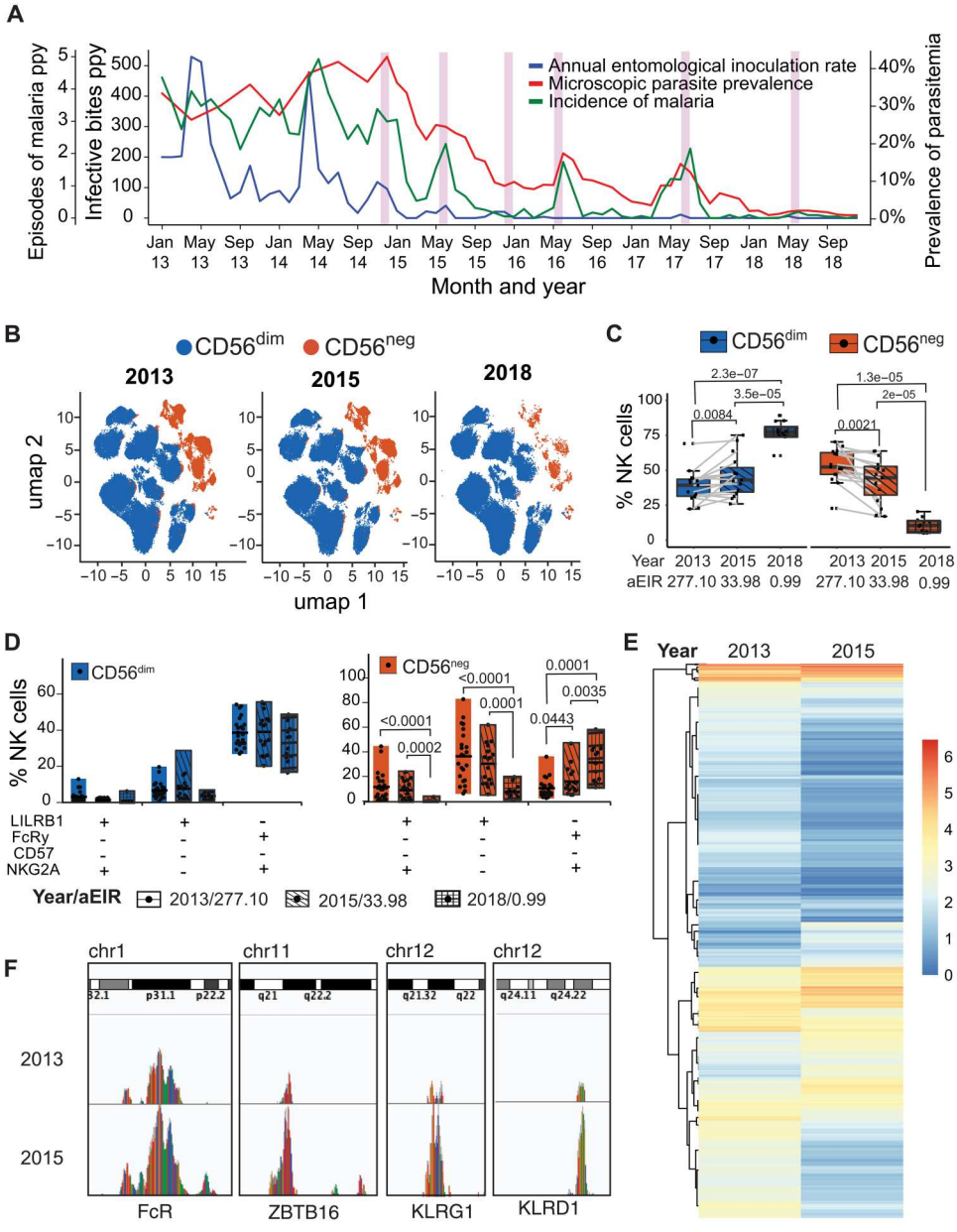

Fig. 6. Decline of CD56^{neg} NK cells after reductions in malaria transmission. (**A**) Measures of malaria burden in Tororo from 2013 to 2018: aEIR (blue, middle *y* axis), malaria incidence (green, left *y* axis), and parasitemia (red, right *y* axis). Pink bars show rounds of indoor residual spraying with insecticides. (**B**) Unsupervised clustering of CD56^{dim} (blue) and CD56^{neg} (red) NK cells within individuals sampled in 2013 and 2015 (paired) and 2018 (unpaired, age-matched), visualized by UMAP projections. (**C**) Percentages of CD56^{dim} and CD56^{neg} NK cells over time as aEIR decreases. (**D**) Proportion of CD56^{dim} (blue) and CD56^{neg} (red) NK cells expressing all possible marker combinations of CD85j, FcRγ, NKG2A, and CD57 plotted over time as aEIR decreases. Clear box indicates 2013, diagonal lined box indicates 2015, and hatched box indicates 2018. (**E**) ATAC-seq heatmap showing differential accessibility of genes from FACS-sorted CD3$^-$CD14$^-$CD19$^-$CD7$^+$ NK cells obtained from a Tororo child sampled in 2013 and 2015. (**F**) ATAC-seq genome tracks showing chromatin accessibility (peaks) at the FcRy, ZBTB16, KLRG1, and KLRD1 loci for 2013 and 2015 paired samples. *P* values for box plots are calculated using Wilcoxon matched-pairs signed rank test. See table S5 for patient characteristics and data file S2 for raw data.

did not significantly change with decreasing malaria transmission (Fig. 6D). However, among CD56^{neg} NK populations, we observed a significant decrease of the LILRB1$^+$, FcRγ$^-$, NKG2A$^{+/-}$, CD57$^-$ NK cells that were predominant in 2013 compared with 2018 ($P < 0.0001$), as well as an increase in the LILRB1$^-$, FcRγ$^+$, NKG2A$^+$, CD57$^-$ NK cells ($P = 0.0001$; Fig. 6D).

The CD56^{neg} populations that decreased were the two most predominant populations that degranulated when stimulated with antibody-opsonized parasites. To determine whether reductions in malaria transmission also altered epigenetic stability of NK cells, we measured chromatin accessibility of sorted NK cells collected in 2013 and 2015 using ATAC-seq. We found that reductions in malaria transmission were associated with global changes in

chromatin accessibility (Fig. 6E). Specifically, accessibility to the promoter regions of FcRγ, ZBTB16, KLRG1, and KLRD1 increased as malaria transmission declined (Fig. 6F). These data suggest that loss of malaria exposure leads to changes in NK cell chromatin accessibility involving genes implicated in NK cell function.

Antibody-mediated cellular cytotoxicity function declines in CD56^{neg} NK cell after decrease in malaria transmission

Last, because we observed changes phenotypically and epigenetically in NK cells after declines in malaria transmission, we evaluated whether there were concomitant changes in NK cell function. We observed a significant decrease of total NK cell degranulation in response to Ugandan plasma–opsonized iRBCs with decreasing malaria transmission (P = 0.0014 comparing 2018 versus 2013; Fig. 7A and fig. S7B), with a stable response to a positive control, anti-RBC–opsonized iRBC (Fig. 7A). Looking more closely at cellular phenotypic subsets, we saw that CD56^{neg} NK cells, but not CD56^{dim} NK cells, exhibited significant reduction of degranulation in response to Ugandan plasma–opsonized iRBCs with decreasing malaria transmission ($P = 8.5 \times 10^{-5}$ in CD56^{neg} NK cells versus P = 0.32 in CD56^{dim} NK comparing 2018 versus 2013; Fig. 7B). Unexpectedly, we observed a similar decline in CD56^{neg}, but not CD56^{dim}, degranulation in response to anti-RBC–opsonized iRBCs (Fig. 7C and fig. S7C). Furthermore, we observed a

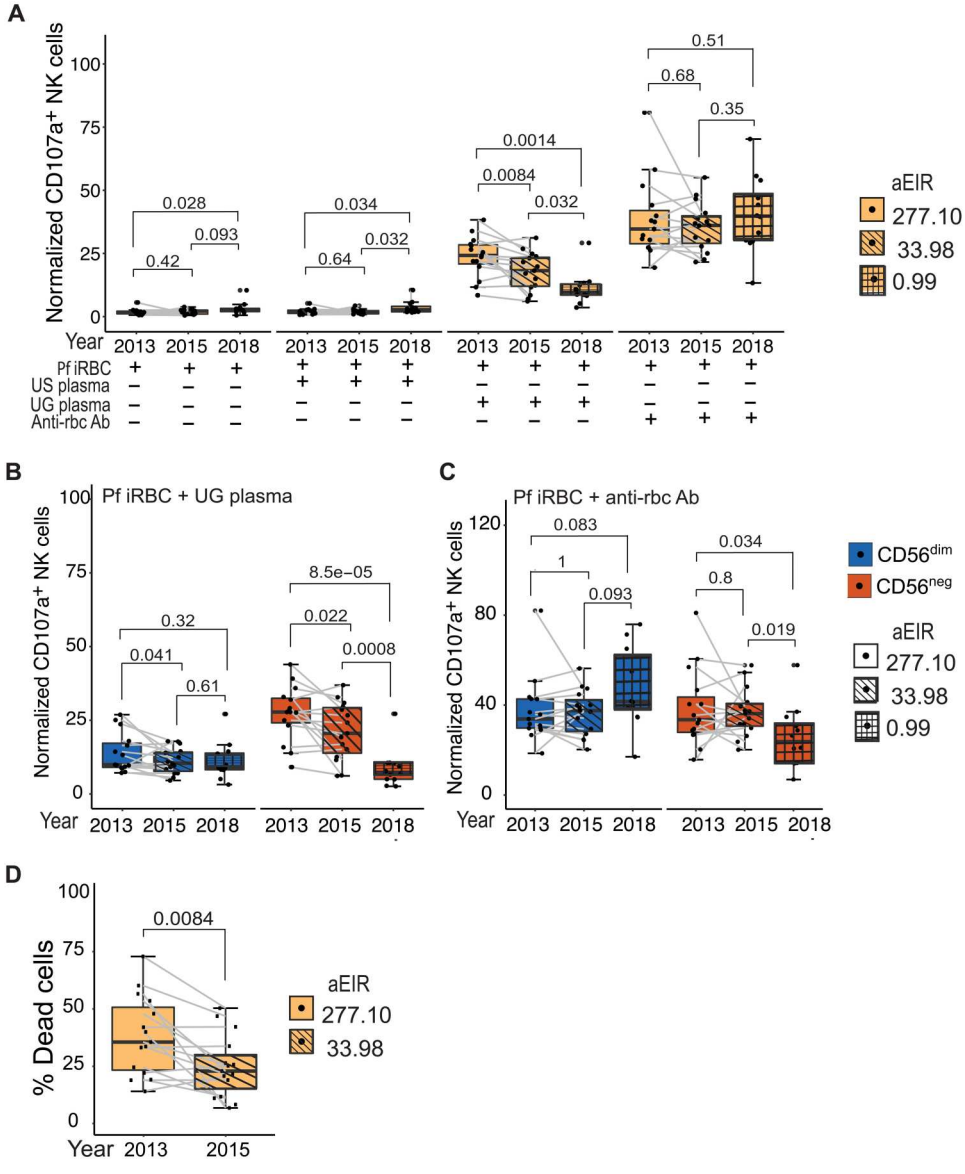

Fig. 7. Reduction of ADCC by CD56^{neg} NK cells after decline of malaria transmission. (**A**) PBMCs were stimulated with iRBCs alone or opsonized with serum. Degranulation was measured through the different years with decreasing aEIR. (**B** and **C**) PBMCs stimulated with iRBCs opsonized with Ugandan serum analyzed by NK cell subset. Degranulation by (B) CD56^{dim} and (C) CD56^{neg} NK cells was measured over time. (**D**) Killing of opsonized p815 cells by PBMCs collected from 2013 and 2015. Clear box indicates 2013 with an aEIR of 258.3, diagonal lined box indicates 2015 with an aEIR of 25.8, and hatched box indicates 2018 with an aEIR of 0.43. *P* values for box plots are calculated using Wilcoxon matched-pairs signed rank test. See table S5 for number of samples and patient characteristics and data file S2 for raw data.

reduced ability to kill antibody-covered p815 cells after IRS (Fig. 7D). Collectively, these data are consistent with the hypothesis that ongoing malaria transmission is required to maintain both the frequency and effector function of CD56^{neg} NK cells. Furthermore, the changing population of CD56^{neg} NK cells in the setting of declining malaria transmission resulted in reduced ADCC activity of NK cells, including both degranulation and killing of target cells.

DISCUSSION

In this study, we characterized the NK cell response among children followed longitudinally across a range of malaria transmission intensities in Uganda. Children repeatedly exposed to malaria had increased frequencies of CD56^{neg} NK cells that resembled CD56^{dim} NK cells transcriptionally, but with several key differences, including decreased expression of PLZF and FcRγ, global histone modifications, and increased protein expression of KIR3DL1 and KIR2DL2/L3/S2, LILRB1, and LAG-3. These CD56^{neg} NK cells were highly functional, displaying greater malaria parasite–induced ADCC than CD56^{dim} NK cells, and higher percentages of these cells were associated with both lower parasite densities and a lower probability of symptomatic disease upon subsequent *Plasmodium* infections. After marked reductions in malaria transmission due to IRS, frequencies—and function—of CD56^{neg} NK cells rapidly declined, suggesting that continuous exposure to malaria is required to maintain this modified, adaptive-like NK cell subset.

Although CD56 is the prototypical identifier of circulating human NK cells (*43*), our data suggest that CD56^{neg} NK cells make up a significant fraction—and in many cases the majority—of circulating NK cells among children living in a high malaria transmission setting. CD56^{neg} NK cells expressed CD7, which has previously been shown to differentiate NK cells from monocyte/dendritic cell–like myeloid cells (*44*, *45*), and transcriptional profiling of PBMCs by CITE-seq confirmed that CD56^{neg} NK cells cluster similarly with CD56^{dim} NK cells. Prior literature has suggested that CD56^{neg} NK cells are dysfunctional and likely represent an exhausted phenotype, given that they have a reduced ability to produce cytokines in response to stimulation (*26*, *28*). We similarly observed that CD56^{neg} cells in malaria-exposed children produce less IFN-γ in response to IL-12/IL-15/IL-18 stimulation than CD56^{dim} NK cells. CD56^{neg} NK cells expressed lower levels of *IL-18RAP*, which likely limits IL-18–mediated cellular activation (*32*), and higher levels of LAG-3, which likely negatively regulates cytokine production in these cells, similar to its role in other NK cells (*34*). We also observed that CD56^{neg} cells express high levels of the inhibitory receptor LILRB1. Recent studies have illuminated that a subset of *Pf* repetitive interspersed repeats (RIFINs), a family of variant surface proteins expressed on the surface of iRBCs, is able to directly bind LILRB1 (*46*, *47*). K562 cells transfected with an LILRB1 binding RIFIN were more resistant to NK cell–mediated lysis than those transfected with a RIFIN unable to bind LILRB1, suggesting that *Pf* RIFIN expression may play a role in immune evasion (*43*). Whether CD56^{neg} NK cells bind *Pf*-RIFIN, and whether this regulates their subsequent activation, remains to be determined.

Along with a reduced response to cytokine stimulation, higher frequencies of CD56^{neg} NK cells were associated with a higher probability of being asymptomatic when subsequently infected with malaria parasites, independent of age and household level transmission intensity. In contrast, CD56^{dim} NK cells were much more inflammatory in vitro, and higher frequencies of these cells were associated with a higher probability of symptoms upon infection. Given the age-dependent inversion of the circulating CD56^{dim} to CD56^{neg} ratio among children living in a high malaria transmission setting, these data are consistent with the hypothesis that epigenetic and transcriptional regulation of the NK cell response is important in limiting the negative consequences of inflammation due to repeated blood-stage malaria.

Despite this reduced response to cytokine stimulation, we observed that CD56^{neg} NK cells potently degranulate in response to opsonized iRBCs and were able to mediate killing of opsonized p815 cells, consistent with a role for these cells having a specialized capacity to perform ADCC. Higher percentages of these cells were also associated with lower parasite densities upon subsequent infection, suggesting an important role of these cells in vivo in mediating anti-parasite immunity. Our data are similar to recently described CD56^{dim} adaptive NK cells, also characterized by low PLZF and FcRγ expression, which were found to have enhanced ADCC against *Pf* iRBCs and were associated with protection against incident malaria (*23*). That study identified NK cells on the basis of CD56 expression and therefore excluded CD56^{neg} NK cells. Given their similar phenotype and function to the CD56^{neg} cells we describe, we suspect significant overlap between adaptive, PLZF^{low}/FcRγ^{low} CD56^{dim} and CD56^{neg} NK cell subsets. Several recent reports have also highlighted specialized antibody-dependent functions of other innate immune cells, including ADCC (*14*) and antibody-dependent phagocytosis (ADP) (*48*) from CD16-expressing γδT cells, as well as ADP from monocytes (*5*, *49*) and neutrophils (*50*). Together, these data suggest that multiple innate immune subsets may be involved in antibody-dependent protection against parasitemia. However, the relative contributions from each subset toward protection—and whether repeated malaria drives epigenetic, transcriptional, and functional remodeling of these cells—remain to be determined.

We show that higher percentages of CD56^{neg} NK cells were observed in children with greater *Pf* exposure and that, after a marked reduction in malaria transmission, both the frequency and function of these cells decline rapidly. Together, these data strongly suggest that continuous exposure to malaria is required to maintain circulating frequencies of CD56^{neg} NK cells. It remains to be determined how malaria drives expansion of these cells and whether these cells represent a clonal, "terminally differentiated" population of NK cells analogous to other effector populations that have been described (*51*) versus expansion of a unique NK cell subset. In contrast to CMV infection, where virally encoded peptides induce expansion of CMV-specific, NKG2C-expressing adaptive NK cells (*52*), our in vitro data do not suggest that CD56^{neg} NK cells respond directly to *Pf* stimulation. Nonetheless, their heightened malaria-specific and nonspecific (e.g., p815 cells) antibody-dependent functionality suggests that these cells play a critical role in innate/adaptive immune bridging.

There were limitations in this study. Not all assays could be performed on all individuals due to sample availability and cost. However, this remains a comprehensive study, leveraging the infrastructure of the East African ICEMR with longitudinal sampling in multiple individuals. Despite their phenotypic, transcriptional, and functional similarity to other NK cells, the ontology of these cells remains unclear, and it is possible that CD56^{neg} NK cells may be

better classified as an alternative innate lymphoid cell subset (*53*). Additional functional characterization of these cells is ongoing. Epidemiological analyses are limited to associations with measure of clinical immunity conditional on participants being infected (i.e., microscopic parasite densities or symptoms if infected). This study is unable to determine whether NK cell subsets are associated with developing a blood-stage infection in the first place nor whether these subsets are associated with protection against submicroscopic parasitemia. Although our data strongly suggest that repeated exposure to malaria results in increased frequencies of $CD56^{neg}$ NK cells, we cannot exclude the possibility that other infections may drive expansion of these cells in this setting. None of the children in this cohort were HIV infected, and nearly all children were CMV seropositive at the time of sampling, precluding comparisons between CMV-seropositive and CMV-seronegative children. Although participants were not tested for EBV, the prevalence of EBV in similar East African settings has been noted to be very high early in life (*54*). Furthermore, associations between aEIR and NK cell phenotypes, and declining percentages of $CD56^{neg}$ NK cells in children after interruptions in malaria transmission, strongly implicate the need for repeated malaria exposure to drive higher frequencies of these cells. Absolute cell counts of NK cell subsets were not available for this cohort. Whereas it is recognized that absolute numbers of peripheral blood lymphocytes and major lymphoid subsets change over the first few years of life, it is unknown whether these changes in cell concentrations are linked to function and/or protection from disease. Last, given the low number of infections after IRS initiation, we were not able to determine whether this immunologic change was associated with a higher propensity for either symptomatic and/or high parasite density infections.

By showing that adaptive-like, functional $CD56^{neg}$ NK cells are associated with anti-disease and anti-parasite protection against malaria, we have identified a clear role of $CD56^{neg}$ NK cells in malaria-endemic settings. Understanding factors that drive programming of this unique NK cell subset will help guide therapeutic translation, including enhancing vaccine-elicited protection. Our findings that these cells are lost in the absence of continuous malaria exposure have important implications regarding maintenance of clinical immunity after interruptions in malaria transmission. It is generally presumed that clinical immunity to malaria is short-lived and wanes rapidly (*3*), due in part to selective and rapid loss of malaria-specific antibodies (*55*). Understanding whether the loss of this cellular immune response plays a role in the resurgence and/or delay of malaria after withdrawal of effective malaria control interventions remains to be determined (*56*). Last, because higher frequencies of $CD56^{neg}$ NK cells have been implicated in the pathogenesis of malignancies, including Burkitt's lymphoma (*27*) and AML (*26*), understanding the impact of these malaria-induced NK cell changes on immune surveillance of malignancy, and responses to other infectious diseases and/or vaccinations, remains critically important.

MATERIALS AND METHODS

Study design

Samples were obtained from children followed longitudinally through the East African ICEMR cohorts in Tororo and Jinja districts (*29*). In these settings, malaria transmission is year-round, with two seasonal peaks and varied transmission intensities (*29*). In Tororo District, before December 2014, malaria control was limited to the distribution of long-lasting insecticide-treated bednets (LLINs) and case management. IRS with the carbamate bendiocarb was first initiated in December 2014, with additional rounds administered in June 2015 and November 2015. In June 2016, IRS was administered with the organophosphate pirimiphos-methyl (Actellic), with repeated rounds in June 2017 and June 2018. IRS was not initiated in Jinja District.

In both sites, all children from 100 randomly selected households were enrolled in the cohort study if they met the following eligibility criteria: (i) documented age between 6 months and less than 10 years, (ii) full-time resident of the household, (iii) no intention to move out of the subcounty for the next 2 years, (iv) agreement to come to a dedicated study clinic located within the subcounty for any febrile illness, (v) agreement to avoid antimalarial medications administered outside the study, and (vi) provision of written informed consent from parent or guardian (*29*). At enrollment, study participants and their parents/guardians were given an LLIN and underwent a standardized evaluation, including evaluation for any chronic medical conditions. No children were found to be HIV-infected.

Children were followed for all care at dedicated study clinics. Those who presented with a fever (tympanic temperature >38.0°C) or history of fever in the previous 24 hours had blood obtained by finger prick for a thick smear. If the thick smear was positive for *Plasmodium* parasites, the patient was diagnosed with malaria regardless of parasite density and was treated with artemether-lumefantrine. Routine assessments, including blood smears to detect for microscopic *Pf* parasitemia, were performed monthly. Participants with asymptomatic parasitemia were not treated with antimalarial drugs in accordance with local guidelines. Household aEIR in the year before sampling was estimated from monthly Centers for Disease Control and Prevention (CDC) light trap mosquito collections. The aEIR was the product of the annual human biting rate (total number of female *Anopheles* mosquitoes captured/number of house nights of collection × 365 days/year) and the sporozoite rate (number of mosquitoes testing positive for *Pf* sporozoites/number of mosquitoes tested). CMV serostatus was measured using the Human Anti-cytomegalovirus IgG ELISA Kit (CMV) ab108724. Regarding KIR genotypes, KIR2DL1 and 3DL1 are present in >98% of Ugandan ICEMR participants (*57*).

Written informed consent was obtained from the parent or guardian of all study participants. The study protocols were approved by the Uganda National Council of Science and Technology (HS 1019), the Makerere University School of Medicine Research and Ethics Committee (2011-167), the University of California, San Francisco Committee on Human Research (11-05995), and the Institutional Review Board at Stanford University (41197).

PBMCs and plasma isolation

At select study visits, 3 to 10 ml of blood were obtained in acid citrate dextrose tubes and/or heparin tubes. Plasma was removed, and PBMCs isolated by density gradient centrifugation (Ficoll-Histopaque; GE Life Sciences) were counted and cryopreserved in liquid nitrogen before shipping to Stanford for downstream analyses. Analysis of cell viability using Guava Viacount (Millipore) consistently demonstrated >90% viability after thaw. Plasma pooled

from 12 adults followed in the high transmission Tororo district or from deidentified plasma from adult U.S. donors was used in ADCC assays. Participant characteristics of samples analyzed in each figure are provided in tables S1 to S5. Data from participants may be represented in more than one figure or table.

NK cell phenotyping

Thawed cells were rested at 37°C for 5 hours, washed with 1× phosphate-buffered saline (PBS), and incubated with cell surface antibodies at room temperature (RT) for 30 min. Cells were washed with fluorescence-activated cell sorting (FACS) buffer [1× PBS with 0.5% bovine serum albumin (BSA) and 0.5 M EDTA], fixed for 15 min (Fix A, Thermo Fisher Scientific), and then permeabilized (Perm B, Thermo Fisher Scientific) before incubation with intracellular antibodies (table S6) for 20 min at RT. Cells were washed with FACS buffer and then resuspended with 1× PBS before analysis on an Attune NXT flow cytometer. Data were analyzed with FlowJo X software (Tree Star).

CITE-seq

The 10X Chromium platform was used to perform CITE-seq. All protocols, including sample preparation, library preparation, and instrument and sequencing settings, are available at https://support.10xgenomics.com/single-cell-gene-expression. About 1,000,000 cells from 10 patient samples were stained with Human TruStain FcX Fc Blocking Reagent (BioLegend, 422302) for 10 min at RT and then stained for 30 min at 4°C. Antibodies and clones used for CITE-seq were anti-human TotalSeq B reagents (BioLegend): TBNK Cocktail, CD7 (CD7-6B7); TCR.Vd2 (B6); CD279 (EH12.2H7); HLADR (L243); CD123 (6H6); CD38 (HB-7); CD57 (QA17A04); CD370 (8F9); CD1c (L161). Cells were then washed twice with PBS supplemented with 2% fetal calf serum and 2 mM EDTA (Sigma-Aldrich) before resuspending in PBS and counting. About 10,000 cells per sample were loaded onto the 10x Chromium controller. Gene expression libraries were prepared for each sample according to the manufacturer's protocol (10x Genomics). Cell surface protein libraries were subjected to double the manufacturer's recommended primer concentration and seven or eight amplification cycles during the sample index polymerase chain reaction (PCR) to reduce the likelihood of daisy chains forming. All libraries were sequenced using NovaSeq 6000 (Illumina) to achieve a minimum of 50,000 paired-end reads per cell for gene expression and 20,000 paired-end reads per cell for cell surface protein libraries.

Epigenetic landscape profiling using cytometry by time of flight

EpiTOF analysis using cytometry by time of flight was performed as previously described (*39*). Briefly, cryopreserved PBMCs were thawed and incubated in RPMI 1640 medium (Thermo Fisher Scientific) containing 10% fetal bovine serum (FBS) (American Type Culture Collection) at 37°C for 1 hour before processing. Cisplatin (ENZO Life Sciences) was added to 10 mM final concentration for viability staining for 5 min before quenching with CyTOF Buffer [PBS (Thermo Fisher Scientific) with 1% BSA (Sigma-Aldrich), 2 mM EDTA (Thermo Fisher Scientific), and 0.05% sodium azide]. Cells were centrifuged at 400*g* for 8 min and stained with lanthanide-labeled antibodies (table S7) against immunophenotypic markers in CyTOF buffer containing Fc receptor blocker (BioLegend) for 30 min at RT. After extracellular marker staining, cells were washed three times with CyTOF buffer and fixed in 1.6% paraformaldehyde (PFA; Electron Microscopy Sciences) at 1×10^6 cells/ml for 15 min at RT. Cells were centrifuged at 600*g* for 5 min after fixation and permeabilized with 1 ml of ice-cold methanol (Thermo Fisher Scientific) for 20 min at 4°C. Four milliliters of CyTOF buffer were added to stop permeabilization. Mass-tag sample barcoding was performed following the manufacturer's protocol (Fluidigm). Individual samples were then combined and stained with intracellular antibodies in CyTOF buffer containing Fc receptor blocker (BioLegend) overnight at 4°C. The following day, cells were washed twice in CyTOF buffer and stained with 250 nM 191/193Ir DNA intercalator (Fluidigm) in PBS with 1.6% PFA for 30 min at RT. Cells were washed twice with CyTOF buffer and once with double-deionized water (ddH_2O) (Thermo Fisher Scientific), followed by filtering through 35-mm strainer to remove aggregates. Cells were resuspended in ddH_2O containing four element calibration beads (Fluidigm) and analyzed on CyTOF2 (Fluidigm).

Assay for transposase-accessible chromatin using sequencing

ATAC-seq analysis was performed as previously described using FAST-ATAC (*58*). In brief, live $CD3^-CD14^-CD19^-CD7^+$ NK cells were sorted into FACS buffer and pelleted by centrifugation at 500*g* relative centrifugal force (RCF) at 4°C in a precooled fixed-angle centrifuge. The supernatant was carefully removed, and 50 μl of transposase mixture [25 μl of 2× tagment DNA (TD) buffer, 2.5 μl of tagment DNA enzyme (TDE1), 0.25 μl of 2% digitonin, and 22.5 μl of nuclease-free water] were added to the cells. After mixing, samples were incubated at 37°C for 30 min in Eppendorf ThermoMixer with agitation at 300 rpm. Transposed DNA was then purified using the QIAGEN MinElute Reaction Cleanup Kit (28204), and purified DNA was eluted in 10 μl of elution buffer (10 mM Tris-HCl, pH 8). Transposed fragments were amplified and purified, and libraries were quantified using quantitative PCR before sequencing. Fast-ATAC libraries were sequenced using paired-end, dual-index library sequencing on an Illumina NextSeq instrument [75–base pair (bp) kit, 36-bp reads, ~20 million to 30 million reads per sample].

Functional assays

Parasite culture and isolation

P. falciparum 3D7 asexual-stage parasites were cultured in RPMI 1640 with 25 mM Hepes, 25 mM sodium bicarbonate, and 1% gentamicin and enriched with 0.5% Albumax (pH 6.75) and 250 μM hypoxanthine under atmospheric conditions (5% oxygen, 5% carbon dioxide, and 95% nitrogen). To retain synchronous cultures, parasite growth was treated with 5% D-sorbitol. Schizont isolation was performed using MACS cell separation LD columns (Miltenyi Biotec) and stored at −80°C. For experiments, schizonts were thawed, washed, and resuspended in RPMI before addition to cells. Mycoplasma contamination was assayed using the MycoAlert Mycoplasma Detection Kit (Lonza).

NK cell isolation

We used the Human NK Cell Isolation Kit (Miltenyi Biotec) to negatively isolate NK cells from freshly thawed PBMCs. First, cells were resuspended with buffer and mixed with NK cell biotin-antibody cocktail for 5 min at 4°C. Then, the provided NK Cell Microbead cocktail was added and incubated for 10 min at 4°C. This was followed by magnetic cell separation using an LS column (Miltenyi

Biotec). Flow-through was collected, washed, and resuspended in R10 [RPMI 1610 (Sigma-Aldrich) with 10% FBS, 1% L-glutamine (Thermo Fisher Scientific), and 1% penicillin and gentamicin (Corning)].

Stimulation assay

Thawed PBMCs were rested for 1 hour at 37°C before the addition of either uninfected RBCs, schizonts, or cytokine cocktail containing recombinant human IL-12 (2.5 ng/ml; R&D Systems), IL-15 (10 ng/ml; PeproTech), and 0.25 μg of IL-18 (R&D Systems). Cultures were incubated for 1 hour at 37°C before addition of protein transport inhibitor brefeldin A (BD). Cells were kept at 37°C for an additional 3 hours before antibody staining (table S6) and analysis on an Attune NXT flow cytometer.

ADCC: Degranulation assay

Freshly thawed schizonts were washed and incubated with RPMI, 10% pooled U.S. plasma, 10% pooled immune Ugandan plasma, or 1:100 anti-RBC (Abcam) at a concentration of 5×10^7 for 1 hour at 37°C. After opsonization, cells were washed and resuspended in R10 (see the "NK cell isolation" section) before mixing with PBMCs or isolated NK cells. CD107a at a dilution of 1:250 (clone H4A3, BioLegend) was immediately added with endoplasmic reticulum (ER) inhibitors—monensin (BD Biosciences) and protein transport inhibitor containing brefeldin A (BD Biosciences). Cells were spun for 3 min at 100*g* before incubating for 5 hours, after which cells were stained and analyzed using the Attune NXT flow cytometer. Data were analyzed with FlowJo X software (Tree Star).

ADCC: p815 killing assay

Killing assay was performed as previously described (*59*) with some modifications. Briefly, p815 cells (a mouse leukemia line) were stained with the CellTrace Violet Cell Proliferation Kit (Thermo Fisher Scientific) at 37°C for 20 min. The reaction was stopped by addition of RPMI (Corning) with 10% FBS at 37°C for 5 min. Stained p815 cells were either opsonized with p815 rat anti-mouse antibody (10 μg/ml; clone: 2.4G2, BD Biosciences) or left uncoated for 30 min at 37°C. After incubation, PBMCs were cocultured with opsonized and uncoated target cells at an effector: target ratio of 10:1. Cocultures were incubated at 37°C for 5 hours before staining for dead and dying cells using 7-aminoactinomycin D (7-AAD) viability staining solution (1:25, BioLegend) and PE annexin V (1:20, Biosciences) in 1× BD Annexin V Binding Buffer for 15 min at RT. Volume was brought up to 200 μl and analyzed on the Attune NXT Flow Cytometer within the hour and analyzed with FlowJo X (Tree Star) software. Percentage of killed target cells was calculated by subtracting the percentages of dead uncoated target cells from the percentages of dead opsonized target cells.

Statistical analysis

All statistical analyses were performed using STATA version 16 (College Station), SPICE v.5.3 (NIAID), Prism 9.0 (GraphPad), or R version 4.2.0. Comparisons of cellular percentages between groups were performed using the Wilcoxon rank sum and/or *t* test, and the Wilcoxon signed-rank test and/or paired *t* test was used to compare paired data. Associations between continuous variables were assessed using Spearman's rank correlation (ρ). Dimensionality reduction was performed with UMAP (*60*). Associations between NK cell tertiles and the monthly probability of symptoms if parasitemic (detected by microscopy), and geometric mean parasite densities if parasitemic, were evaluated using multilevel mixed-effects models. These analyses accounted for repeated measures within individuals and were clustered on household to account for multiple children living in the same household. In multivariate analyses, odds ratios for symptoms when infected were adjusted for age and aEIR. Two-sided *P* values were calculated for all test statistics, and $P < 0.05$ was considered significant.

CITE-seq analysis

Droplet libraries were processed using Cell Ranger v4.0. Reads were aligned to the GRCh38 human genome using STAR (v2.5.1b), and unique molecular identifiers (UMIs) were deduplicated. Antibody-derived tag counts for each protein were first normalized using counts per million and log-transformed, with a pseudocount of +1. To estimate the background signal for each protein, we fit a two-component Gaussian mixture model, implemented in the R package function "mclust" (v5.4.7), across the droplets with a total UMI count of >10 and <100 from each experimental sample separately. The mean of the first Gaussian mixture model component for each protein was then subtracted from the log counts per million from the quality control–passed droplets in the respective experimental sample. Raw data were filtered to remove cells that expressed fewer than 200 genes and >10% mitochondrial reads. We used the variable stabilization transformation from the Seurat R package (*61*) to integrate and transform the count data into normalized and scaled data that can be used for downstream analysis.

We used UMAP for dimensionality reduction and data visualization, the Louvain algorithm to identify cell clusters, and the singleR package to annotate cell clusters by comparing transcriptomic profiles between cell clusters and reference data from the Human Primary Cell Atlas (*62*). We manually gated protein-level expression data to identify three NK cell subsets, including $CD56^{neg}$ ($CD19^-$ $CD3^-$ $CD14^-$ $CD7^+$ $CD16^+$ $CD56^-$), $CD56^{dim}$ ($CD19^-$ $CD3^-$ $CD14^-$ $CD7^+$ $CD16^+$ $CD56^{dim}$), and $CD56^{bright}$ NK cells ($CD19^-$ $CD3^-$ $CD14^-$ $CD7^+$ $CD16^-$ $CD56^+$), and these subsets were mapped to the UMAP projection. We performed likelihood ratio tests [implemented as the FindMarkers function in the Seurat R package (*61*)] to identify differentially expressed genes between $CD56^-$ NK cells and $CD56^{dim}$ NK cells.

EpiTOF analysis

Raw data were preprocessed using FlowJo to identify cell events from individual samples by palladium-based mass tags and to segregate specific immune cell populations by immunophenotypic markers (gating hierarchy in fig. S3). Single-cell data for various immune cell subtypes from individual participants were exported from FlowJo for downstream computational analyses. The exported FlowJo data were then analyzed following previously reported methods (*39*). In brief, the value of each histone mark was regressed against the total amount of histones, represented by measured values of H3 and H4. For sample-level analyses, the values of each histone mark were averaged for each cell type in each sample. Distances of epigenetic profiles of NK cell types were obtained by computing Euclidean distances from the centers of the epigenetic profiles for each cell type. Statistical significance of the differences between groups at the sample level was assessed by computing an effect size with Hedges' *g* formula, and *P* values were corrected for multiple comparisons with the Benjamini-Hochberg method.

ATAC-seq analysis

We used ChrAccR, an R package for comprehensive analysis of chromatin accessibility data (https://greenleaflab.github.io/ChrAccR/). We identified open chromatin peaks that varied

across the different time points from the same child and that are differentially enriched for transcription factor binding motifs in regulatory elements (e.g., gene promoters and distal enhancers). Specific sites of interest were visualized with Integrative Genome Viewer (Broad Institute, Cambridge, MA).

Supplementary Materials

This PDF file includes:
Figs. S1 to S7
Tables S1 to S7

Other Supplementary Material for this manuscript includes the following:
Data file S1 and S2

View/request a protocol for this paper from *Bio-protocol*.

REFERENCES AND NOTES

1. World Health Organization, *World Malaria Report 2021* (World Health Organization, 2021).
2. I. Rodriguez-Barraquer, E. Arinaitwe, P. Jagannathan, M. R. Kamya, P. J. Rosenthal, J. Rek, G. Dorsey, J. Nankabirwa, S. G. Staedke, M. Kilama, C. Drakeley, I. Ssewanyana, D. L. Smith, B. Greenhouse, Quantification of anti-parasite and anti-disease immunity to malaria as a function of age and exposure. *eLife* **7**, (2018).
3. J. Langhorne, F. M. Ndungu, A. M. Sponaas, K. Marsh, Immunity to malaria: More questions than answers. *Nat. Immunol.* **9**, 725–732 (2008).
4. J. Tan, L. Piccoli, A. Lanzavecchia, The antibody response to *Plasmodium falciparum*: Cues for vaccine design and the discovery of receptor-based antibodies. *Annu. Rev. Immunol.* **37**, 225–246 (2018).
5. F. H. Osier, G. Feng, M. J. Boyle, C. Langer, J. Zhou, J. S. Richards, F. J. McCallum, L. Reiling, A. Jaworowski, R. F. Anders, K. Marsh, J. G. Beeson, Opsonic phagocytosis of Plasmodium falciparum merozoites: Mechanism in human immunity and a correlate of protection against malaria. *BMC Med.* **12**, 108 (2014).
6. M. J. Boyle, L. Reiling, G. Feng, C. Langer, F. H. Osier, H. Aspeling-Jones, Y. S. Cheng, J. Stubbs, K. K. Tetteh, D. J. Conway, J. S. McCarthy, I. Muller, K. Marsh, R. F. Anders, J. G. Beeson, Human antibodies fix complement to inhibit Plasmodium falciparum invasion of erythrocytes and are associated with protection against malaria. *Immunity* **42**, 580–590 (2015).
7. G. Arora, G. T. Hart, J. Manzella-Lapeira, J. Y. Doritchamou, D. L. Narum, L. M. Thomas, J. Brzostowski, S. Rajagopalan, O. K. Doumbo, B. Traore, L. H. Miller, S. K. Pierce, P. E. Duffy, P. D. Crompton, S. A. Desai, E. O. Long, NK cells inhibit Plasmodium falciparum growth in red blood cells via antibody-dependent cellular cytotoxicity. *eLife* **7**, (2018).
8. M. M. Stevenson, E. M. Riley, Innate immunity to malaria. *Nat. Rev. Immunol.* **4**, 169–180 (2004).
9. C. L. Chua, G. Brown, J. A. Hamilton, S. Rogerson, P. Boeuf, Monocytes and macrophages in malaria: Protection or pathology? *Trends Parasitol.* **29**, 26–34 (2013).
10. E. M. Riley, P. H. Jakobsen, S. J. Allen, J. G. Wheeler, S. Bennett, S. Jepsen, B. M. Greenwood, Immune response to soluble exoantigens of Plasmodium falciparum may contribute to both pathogenesis and protection in clinical malaria: Evidence from a longitudinal, prospective study of semi-immune African children. *Eur. J. Immunol.* **21**, 1019–1025 (1991).
11. P. Jagannathan, C. C. Kim, B. Greenhouse, F. Nankya, K. Bowen, I. Eccles-James, M. K. Muhindo, E. Arinaitwe, J. W. Tappero, M. R. Kamya, G. Dorsey, M. E. Feeney, Loss and dysfunction of V$\delta2^+$ $\gamma\delta$ T cells are associated with clinical tolerance to malaria. *Sci. Transl. Med.* **6**, 251ra117 (2014).
12. P. Jagannathan, F. Lutwama, M. J. Boyle, F. Nankya, L. A. Farrington, T. I. McIntyre, K. Bowen, K. Naluwu, M. Nalubega, K. Musinguzi, E. Sikyomu, R. Budker, A. Katureebe, J. Rek, B. Greenhouse, G. Dorsey, M. R. Kamya, M. E. Feeney, V$\delta2$+ T cell response to malaria correlates with protection from infection but is attenuated with repeated exposure. *Sci. Rep.* **7**, 11487 (2017).
13. R. Guha, A. Mathioudaki, S. Doumbo, D. Doumtabe, J. Skinner, G. Arora, S. Siddiqui, S. Li, K. Kayentao, A. Ongoiba, J. Zaugg, B. Traore, P. D. Crompton, Plasmodium falciparum malaria drives epigenetic reprogramming of human monocytes toward a regulatory phenotype. *PLOS Pathog.* **17**, e1009430 (2021).
14. L. A. Farrington, P. C. Callaway, H. M. Vance, K. Baskevitch, E. Lutz, L. Warrier, T. I. McIntyre, R. Budker, P. Jagannathan, F. Nankya, K. Musinguzi, M. Nalubega, E. Sikyomu, K. Naluwu, E. Arinaitwe, G. Dorsey, M. R. Kamya, M. E. Feeney, Opsonized antigen activates V$\delta2$+ T cells via CD16/FCγRIIIa in individuals with chronic malaria exposure. *PLOS Pathog.* **16**, e1008997 (2020).
15. J. Walk, L. C. J. de Bree, W. Graumans, R. Stoter, G. J. van Gemert, M. van de Vegte-Bolmer, K. Teelen, C. C. Hermsen, R. J. W. Arts, M. C. Behet, F. Keramati, S. Moorlag, A. S. P. Yang, R. van Crevel, P. Aaby, Q. de Mast, A. van der Ven, C. Stabell Benn, M. G. Netea, R. W. Sauerwein, Outcomes of controlled human malaria infection after BCG vaccination. *Nat. Commun.* **10**, 874 (2019).
16. K. R. Dobbs, P. Embury, J. Vulule, P. S. Odada, B. A. Rosa, M. Mitreva, J. W. Kazura, A. E. Dent, Monocyte dysregulation and systemic inflammation during pediatric falciparum malaria. *JCI Insight* **2**, (2017).
17. J. N. Crabtree, D. R. Caffrey, L. de Souza Silva, E. A. Kurt-Jones, K. Dobbs, A. Dent, K. A. Fitzgerald, D. T. Golenbock, Lymphocyte crosstalk is required for monocyte-intrinsic trained immunity to Plasmodium falciparum. *J. Clin. Invest.* **132**, (2022).
18. K. Artavanis-Tsakonas, E. M. Riley, Innate immune response to malaria: Rapid induction of IFN-gamma from human NK cells by live Plasmodium falciparum-infected erythrocytes. *J. Immunol.* **169**, 2956–2963 (2002).
19. A. S. Wolf, S. Sherratt, E. M. Riley, NK cells: Uncertain allies against malaria. *Front. Immunol.* **8**, 212 (2017).
20. A. Horowitz, D. M. Strauss-Albee, M. Leipold, J. Kubo, N. Nemat-Gorgani, O. C. Dogan, C. L. Dekker, S. Mackey, H. Maecker, G. E. Swan, M. M. Davis, P. J. Norman, L. A. Guethlein, M. Desai, P. Parham, C. A. Blish, Genetic and environmental determinants of human NK cell diversity revealed by mass cytometry. *Sci. Transl. Med.* **5**, 208ra145 (2013).
21. D. M. Strauss-Albee, J. Fukuyama, E. C. Liang, Y. Yao, J. A. Jarrell, A. L. Drake, J. Kinuthia, R. R. Montgomery, G. John-Stewart, S. Holmes, C. A. Blish, Human NK cell repertoire diversity reflects immune experience and correlates with viral susceptibility. *Sci. Transl. Med.* **7**, 297ra115 (2015).
22. C. Yang, J. R. Siebert, R. Burns, Z. J. Gerbec, B. Bonacci, A. Rymaszewski, M. Rau, M. J. Riese, S. Rao, K. S. Carlson, J. M. Routes, J. W. Verbsky, M. S. Thakar, S. Malarkannan, Heterogeneity of human bone marrow and blood natural killer cells defined by single-cell transcriptome. *Nat. Commun.* **10**, 3931 (2019).
23. G. T. Hart, T. M. Tran, J. Theorell, H. Schlums, G. Arora, S. Rajagopalan, A. D. J. Sangala, K. J. Welsh, B. Traore, S. K. Pierce, P. D. Crompton, Y. T. Bryceson, E. O. Long, Adaptive NK cells in people exposed to Plasmodium falciparum correlate with protection from malaria. *J. Exp. Med.* **216**, 1280–1290 (2019).
24. D. Mavilio, G. Lombardo, J. Benjamin, D. Kim, D. Follman, E. Marcenaro, M. A. O'Shea, A. Kinter, C. Kovacs, A. Moretta, A. S. Fauci, Characterization of CD56-/CD16+ natural killer (NK) cells: A highly dysfunctional NK subset expanded in HIV-infected viremic individuals. *Proc. Natl. Acad. Sci. U.S.A.* **102**, 2886–2891 (2005).
25. V. D. Gonzalez, K. Falconer, N. K. Bjorkstrom, K. G. Blom, O. Weiland, H. G. Ljunggren, A. Alaeus, J. K. Sandberg, Expansion of functionally skewed CD56-negative NK cells in chronic hepatitis C virus infection: Correlation with outcome of pegylated IFN-alpha and ribavirin treatment. *J. Immunol.* **183**, 6612–6618 (2009).
26. A. S. Chretien, R. Devillier, S. Granjeaud, C. Cordier, C. Demerle, N. Salem, J. Wlosik, F. Orlanducci, L. Gorvel, S. Fattori, M. A. Hospital, J. Pakradouni, E. Gregori, M. Paul, P. Rochigneux, T. Pagliardini, M. Morey, C. Fauriat, N. Dulphy, A. Toubert, H. Luche, M. Malissen, D. Blaise, J. A. Nunes, N. Vey, D. Olive, High-dimensional mass cytometry analysis of NK cell alterations in AML identifies a subgroup with adverse clinical outcome. *Proc. Natl. Acad. Sci. U.S.A.* **118**, (2021).
27. C. S. Forconi, C. P. Cosgrove, P. Saikumar-Lakshmi, C. E. Nixon, J. Foley, J. M. Ong'echa, J. A. Otieno, G. Alter, C. Munz, A. M. Moormann, Poorly cytotoxic terminally differentiated CD56^{neg}CD16^{pos} NK cells accumulate in Kenyan children with Burkitt lymphomas. *Blood Adv.* **2**, 1101–1114 (2018).
28. N. K. Bjorkstrom, H. G. Ljunggren, J. K. Sandberg, CD56 negative NK cells: Origin, function, and role in chronic viral disease. *Trends Immunol.* **31**, 401–406 (2010).
29. M. R. Kamya, E. Arinaitwe, H. Wanzira, A. Katureebe, C. Barusya, S. P. Kigozi, M. Kilama, A. J. Tatem, P. J. Rosenthal, C. Drakeley, S. W. Lindsay, S. G. Staedke, D. L. Smith, B. Greenhouse, G. Dorsey, Malaria transmission, infection, and disease at three sites with varied transmission intensity in Uganda: Implications for malaria control. *Am. J. Trop. Med. Hyg.* **92**, 903–912 (2015).
30. T. D. Holmes, R. V. Pandey, E. Y. Helm, H. Schlums, H. Han, T. M. Campbell, T. T. Drashansky, S. Chiang, C. Y. Wu, C. Tao, M. Shoukier, E. Tolosa, S. Von Hardenberg, M. Sun, C. Klemann, R. A. Marsh, C. M. Lau, Y. Lin, J. C. Sun, R. Mansson, F. Cichocki, D. Avram, Y. T. Bryceson, The transcription factor Bcl11b promotes both canonical and adaptive NK cell differentiation. *Sci. Immunol.* **6**, (2021).
31. D. Brownlie, M. Scharenberg, J. E. Mold, J. Hard, E. Kekalainen, M. Buggert, S. Nguyen, J. N. Wilson, M. Al-Ameri, H. G. Ljunggren, N. Marquardt, J. Michaelsson, Expansions of adaptive-like NK cells with a tissue-resident phenotype in human lung and blood. *Proc. Natl. Acad. Sci. U.S.A.* **118**, (2021).
32. T. L. Born, E. Thomassen, T. A. Bird, J. E. Sims, Cloning of a novel receptor subunit, AcPL, required for interleukin-18 signaling. *J. Biol. Chem.* **273**, 29445–29450 (1998).
33. S. Narayanan, P. J. Ahl, V. A. Bijin, N. Kaliaperumal, S. G. Lim, C.-I. Wang, A.-M. Fairhurst, J. E. Connolly, LAG3 is a central regulator of NK cell cytokine production. bioRxiv

2020.01.31.928200 [Preprint]. 2 February 2020. https://doi.org/10.1101/2020.01.31.928200.
34. A. Merino, B. Zhang, P. Dougherty, X. Luo, J. Wang, B. R. Blazar, J. S. Miller, F. Cichocki, Chronic stimulation drives human NK cell dysfunction and epigenetic reprograming. *J. Clin. Invest.* **129**, 3770–3785 (2019).
35. A. C. Anderson, N. Joller, V. K. Kuchroo, Lag-3, Tim-3, and TIGIT: Co-inhibitory receptors with specialized functions in immune regulation. *Immunity* **44**, 989–1004 (2016).
36. S. L. Smith, P. R. Kennedy, K. B. Stacey, J. D. Worboys, A. Yarwood, S. Seo, E. H. Solloa, B. Mistretta, S. S. Chatterjee, P. Gunaratne, K. Allette, Y. C. Wang, M. L. Smith, R. Sebra, E. M. Mace, A. Horowitz, W. Thomson, P. Martin, S. Eyre, D. M. Davis, Diversity of peripheral blood human NK cells identified by single-cell RNA sequencing. *Blood Adv.* **4**, 1388–1406 (2020).
37. N. K. Bjorkstrom, P. Riese, F. Heuts, S. Andersson, C. Fauriat, M. A. Ivarsson, A. T. Bjorklund, M. Flodstrom-Tullberg, J. Michaelsson, M. E. Rottenberg, C. A. Guzman, H. G. Ljunggren, K. J. Malmberg, Expression patterns of NKG2A, KIR, and CD57 define a process of CD56dim NK-cell differentiation uncoupled from NK-cell education. *Blood* **116**, 3853–3864 (2010).
38. H. Schlums, F. Cichocki, B. Tesi, J. Theorell, V. Beziat, T. D. Holmes, H. Han, S. C. Chiang, B. Foley, K. Mattsson, S. Larsson, M. Schaffer, K. J. Malmberg, H. G. Ljunggren, J. S. Miller, Y. T. Bryceson, Cytomegalovirus infection drives adaptive epigenetic diversification of NK cells with altered signaling and effector function. *Immunity* **42**, 443–456 (2015).
39. P. Cheung, F. Vallania, H. C. Warsinske, M. Donato, S. Schaffert, S. E. Chang, M. Dvorak, C. L. Dekker, M. M. Davis, P. J. Utz, P. Khatri, A. J. Kuo, Single-cell chromatin modification profiling reveals increased epigenetic variations with aging. *Cell* **173**, 1385–1397.e14 (2018).
40. C. Cruz, M. Della Rosa, C. Krueger, Q. Gao, D. Horkai, M. King, L. Field, J. Houseley, Trimethylation of histone H3 lysine 4 facilitates gene expression in ageing cells. *eLife* **7**, (2018).
41. I. Hwang, T. Zhang, J. M. Scott, A. R. Kim, T. Lee, T. Kakarla, A. Kim, J. B. Sunwoo, S. Kim, Identification of human NK cells that are deficient for signaling adaptor FcRγ and specialized for antibody-dependent immune functions. *Int. Immunol.* **24**, 793–802 (2012).
42. J. I. Nankabirwa, E. Arinaitwe, J. Rek, M. Kilama, T. Kizza, S. G. Staedke, P. J. Rosenthal, I. Rodriguez-Barraquer, J. Briggs, B. Greenhouse, T. Bousema, C. Drakeley, D. S. Roos, S. S. Tomko, D. L. Smith, M. R. Kamya, G. Dorsey, Malaria transmission, infection, and disease following sustained indoor residual spraying of insecticide in Tororo, Uganda. *Am. J. Trop. Med. Hyg.* **103**, 1525–1533 (2020).
43. M. A. Caligiuri, Human natural killer cells. *Blood* **112**, 461–469 (2008).
44. J. M. Milush, B. R. Long, J. E. Snyder-Cappione, A. J. Cappione III, V. A. York, L. C. Ndhlovu, L. L. Lanier, J. Michaelsson, D. F. Nixon, Functionally distinct subsets of human NK cells and monocyte/DC-like cells identified by coexpression of CD56, CD7, and CD4. *Blood* **114**, 4823–4831 (2009).
45. J. M. Milush, S. Lopez-Verges, V. A. York, S. G. Deeks, J. N. Martin, F. M. Hecht, L. L. Lanier, D. F. Nixon, CD56negCD16(+) NK cells are activated mature NK cells with impaired effector function during HIV-1 infection. *Retrovirology* **10**, 158 (2013).
46. F. Saito, K. Hirayasu, T. Satoh, C. W. Wang, J. Lusingu, T. Arimori, K. Shida, N. M. Q. Palacpac, S. Itagaki, S. Iwanaga, E. Takashima, T. Tsuboi, M. Kohyama, T. Suenaga, M. Colonna, J. Takagi, T. Lavstsen, T. Horii, H. Arase, Immune evasion of Plasmodium falciparum by RIFIN via inhibitory receptors. *Nature* **552**, 101–105 (2017).
47. Y. Chen, K. Xu, L. Piccoli, M. Foglierini, J. Tan, W. Jin, J. Gorman, Y. Tsybovsky, B. Zhang, B. Traore, C. Silacci-Fregni, C. Daubenberger, P. D. Crompton, R. Geiger, F. Sallusto, P. D. Kwong, A. Lanzavecchia, Structural basis of malaria RIFIN binding by LILRB1-containing antibodies. *Nature* **592**, 639–643 (2021).
48. C. Junqueira, R. B. Polidoro, G. Castro, S. Absalon, Z. Liang, S. Sen Santara, A. Crespo, D. B. Pereira, R. T. Gazzinelli, J. D. Dvorin, J. Lieberman, γδ T cells suppress *Plasmodium falciparum* blood-stage infection by direct killing and phagocytosis. *Nat. Immunol.* **22**, 347–357 (2021).
49. F. K. Musasia, I. N. Nkumama, R. Frank, V. Kipkemboi, M. Schneider, K. Mwai, D. O. Odera, M. Rosenkranz, K. Furle, D. Kimani, J. Tuju, P. Njuguna, M. Hamaluba, M. C. Kapulu, H. Wardemann; CHMI-SIKA Study Team, F. H. A. Osier, Phagocytosis of *Plasmodium falciparum* ring-stage parasites predicts protection against malaria. *Nat. Commun.* **13**, 4098 (2022).
50. A. Garcia-Senosiain, I. H. Kana, S. Singh, M. K. Das, M. H. Dziegiel, S. Hertegonne, B. Adu, M. Theisen, Neutrophils dominate in opsonic phagocytosis of P. falciparum blood-stage merozoites and protect against febrile malaria. *Commun. Biol.* **4**, 984 (2021).
51. N. Huot, P. Rascle, C. Petitdemange, V. Contreras, C. M. Sturzel, E. Baquero, J. L. Harper, C. Passaes, R. Legendre, H. Varet, Y. Madec, U. Sauermann, C. Stahl-Hennig, J. Nattermann, A. Saez-Cirion, R. Le Grand, R. Keith Reeves, M. Paiardini, F. Kirchhoff, B. Jacquelin, M. Muller-Trutwin, SIV-induced terminally differentiated adaptive NK cells in lymph nodes associated with enhanced MHC-E restricted activity. *Nat. Commun.* **12**, 1282 (2021).
52. Q. Hammer, T. Ruckert, E. M. Borst, J. Dunst, A. Haubner, P. Durek, F. Heinrich, G. Gasparoni, M. Babic, A. Tomic, G. Pietra, M. Nienen, I. W. Blau, J. Hofmann, I. K. Na, I. Prinz, C. Koenecke, P. Hemmati, N. Babel, R. Arnold, J. Walter, K. Thurley, M. F. Mashreghi, M. Messerle, C. Romagnani, Peptide-specific recognition of human cytomegalovirus strains controls adaptive natural killer cells. *Nat. Immunol.* **19**, 453–463 (2018).
53. Y. Simoni, M. Fehlings, H. N. Kloverpris, N. McGovern, S. L. Koo, C. Y. Loh, S. Lim, A. Kurioka, J. R. Fergusson, C. L. Tang, M. H. Kam, K. Dennis, T. K. H. Lim, A. C. Y. Fui, C. W. Hoong, J. K. Y. Chan, M. Curotto de Lafaille, S. Narayanan, S. Baig, M. Shabeer, S. E. S. Toh, H. K. K. Tan, R. Anicete, E. H. Tan, A. Takano, P. Klenerman, A. Leslie, D. S. W. Tan, I. B. Tan, F. Ginhoux, E. W. Newell, Human innate lymphoid cell subsets possess tissue-type based heterogeneity in phenotype and frequency. *Immunity* **46**, 148–161 (2017).
54. E. Piriou, A. S. Asito, P. O. Sumba, N. Fiore, J. M. Middeldorp, A. M. Moormann, R. Ploutz-Snyder, R. Rochford, Early age at time of primary Epstein-Barr virus infection results in poorly controlled viral infection in infants from Western Kenya: Clues to the etiology of endemic Burkitt lymphoma. *J. Infect. Dis.* **205**, 906–913 (2012).
55. I. Ssewanyana, J. Rek, I. Rodriguez, L. Wu, E. Arinaitwe, J. I. Nankabirwa, J. G. Beeson, H. Mayanja-Kizza, P. J. Rosenthal, G. Dorsey, M. R. Kamya, C. Drakeley, B. Greenhouse, K. K. A. Tetteh, Impact of a rapid decline in Malaria transmission on antimalarial IgG subclasses and avidity. *Front. Immunol.* **11**, 576663 (2020).
56. B. Greenwood, I. Zongo, A. Dicko, D. Chandramohan, R. W. Snow, C. Ockenhouse, Resurgent and delayed malaria. *Malar. J.* **21**, 77 (2022).
57. J. C. Digitale, P. C. Callaway, M. Martin, G. Nelson, M. Viard, J. Rek, E. Arinaitwe, G. Dorsey, M. Kamya, M. Carrington, I. Rodriguez-Barraquer, M. E. Feeney, Association of inhibitory killer cell immunoglobulin-like receptor ligands with higher Plasmodium falciparum parasite prevalence. *J. Infect. Dis.* **224**, 175–183 (2021).
58. M. R. Corces, J. D. Buenrostro, B. Wu, P. G. Greenside, S. M. Chan, J. L. Koenig, M. P. Snyder, J. K. Pritchard, A. Kundaje, W. J. Greenleaf, R. Majeti, H. Y. Chang, Lineage-specific and single-cell chromatin accessibility charts human hematopoiesis and leukemia evolution. *Nat. Genet.* **48**, 1193–1203 (2016).
59. R. Roy Chowdhury, F. Vallania, Q. Yang, C. J. Lopez Angel, F. Darboe, A. Penn-Nicholson, V. Rozot, E. Nemes, S. T. Malherbe, K. Ronacher, G. Walzl, W. Hanekom, M. M. Davis, J. Winter, X. Chen, T. J. Scriba, P. Khatri, Y. H. Chien, A multi-cohort study of the immune factors associated with *M. tuberculosis* infection outcomes. *Nature* **560**, 644–648 (2018).
60. L. McInnes, J. Healy, J. Melville, UMAP: Uniform manifold approximation and projection for dimension reduction. arXiv:1802.03426 [stat.ML] (9 February 2018).
61. Y. Hao, S. Hao, E. Andersen-Nissen, W. M. Mauck III, S. Zheng, A. Butler, M. J. Lee, A. J. Wilk, C. Darby, M. Zager, P. Hoffman, M. Stoeckius, E. Papalexi, E. P. Mimitou, J. Jain, A. Srivastava, T. Stuart, L. M. Fleming, B. Yeung, A. J. Rogers, J. M. McElrath, C. A. Blish, R. Gottardo, P. Smibert, R. Satija, Integrated analysis of multimodal single-cell data. *Cell* **184**, 3573–3587.e29 (2021).
62. N. A. Mabbott, J. K. Baillie, H. Brown, T. C. Freeman, D. A. Hume, An expression atlas of human primary cells: Inference of gene function from coexpression networks. *BMC Genomics* **14**, 632 (2013).

Acknowledgments: We are grateful to all the parents and guardians for giving their consent and to the study participants for their cooperation. We thank all the members of the study team for their tireless effort and excellent work. **Funding:** Support for this work was provided by the following grants: NIH grants U01AI150741 (to B.G. and P.J.), R01AI093615 (to M.F.), and U19AI089674 (to G.D. and M.K.); Australian National Health and Medical Research Council Ideas Grant CIA GNT1181932 and Career Development Fellowship 1 GNT1141632 (to M.B.); and Bill and Melinda Gates Foundation/Stanford Center for Human Systems Immunology (OPP 1113682, Pilot Project to P.J.). **Author contributions:** M.T. and P.J. conceptualized the study, and P.J. provided study supervision. M.T., S.S., P.C.C., J.R., K.D.P., K.v.d.P., J.N., Z.H., S.K., W.G., M.D., S. Tukwasibwe, E.A., F.N., K.M., D.A., L.d.l.P., D.M.M., S.N.L., S. Takahashi, I.R.B., C.B., P.J.U., P.K., G.D., M.K., M.B., M.F., I.S., and P.J. designed or performed experiments and analyzed data. M.T., S.S., K.D.P., J.N., Z.H., I.R.B., and P.J. generated figures and visualizations. W.G., P.J.U., P.K., G.D., M.K., M.B., M.F., and .P.J. provided funding for the study. J.R., E.A., M.K., and I.S. coordinated the clinical study and participant sampling. M.T. and P.J. wrote the original draft, and M.T., S.S., P.C.C., J.R., K.D.P., K.v.d.P., J.N., Z.H., S.K., W.G., M.D., S. Tukwasibwe, E.A., F.N., K.M., D.A., L.d.l.P., D.M.M., S.N.L., S. Takahashi, I.R.B., B.G., C.B., P.J.U., P.K., G.D., M.K., M.B., M.F., I.S., and P.J. edited the manuscript. **Competing interests:** The authors declare that they have no competing interests. **Data and materials availability:** All data associated with this study are present in the paper or the Supplementary Materials. Raw data from figures with $n < 25$ observations are in data file S2. RNA and ATAC sequencing data have been deposited at NCBI Gene Expression Omnibus under accession number GSE210943 and are publicly available (www.ncbi.nlm.nih.gov/geo/query/acc.cgi?acc=GSE210943). Clinical data from both study cohorts are fully accessible online via the ClinepiDB platform (clinepidb.org, "PRISM" studies), at the level of the cohort, household, individual, and visit.

Submitted 12 July 2022
Accepted 5 January 2023
Published 25 January 2023
10.1126/scitranslmed.add9012

Science Translational Medicine

Malaria-driven expansion of adaptive-like functional CD56-negative NK cells correlates with clinical immunity to malaria

Maureen Ty, Shenghuan Sun, Perri C. Callaway, John Rek, Kathleen D. Press, Kattria van der Ploeg, Jason Nideffer, Zicheng Hu, Sandy Klemm, William Greenleaf, Michele Donato, Stephen Tukwasibwe, Emmanuel Arinaitwe, Felistas Nankya, Kenneth Musinguzi, Dean Andrew, Lauren de la Parte, Diego Martinez Mori, Savannah N. Lewis, Saki Takahashi, Isabel Rodriguez-Barraquer, Bryan Greenhouse, Catherine Blish, PJ Utz, Purvesh Khatri, Grant Dorsey, Moses Kamya, Michelle Boyle, Margaret Feeney, Isaac Ssewanyana, and Prasanna Jagannathan

Sci. Transl. Med., **15** (680), eadd9012.
DOI: 10.1126/scitranslmed.add9012